



**QUEEN'S  
UNIVERSITY  
BELFAST**

## Design of a novel 5-DOF flexure-based compound alignment stage for Roll-to-Roll Printed Electronics

Chen, W., Yang, S., Liu, J., Chen, W., & Jin, Y. (2017). Design of a novel 5-DOF flexure-based compound alignment stage for Roll-to-Roll Printed Electronics. *Review of Scientific Instruments*, 88, [025002].  
<https://doi.org/10.1063/1.4974814>

**Published in:**  
Review of Scientific Instruments

**Document Version:**  
Peer reviewed version

**Queen's University Belfast - Research Portal:**  
[Link to publication record in Queen's University Belfast Research Portal](#)

### **Publisher rights**

Copyright AIP Publishing 2017

This article may be downloaded for personal use only. Any other use requires prior permission of the author and AIP Publishing.

The following article appeared in Review of Scientific Instruments and may be found at (<http://aip.scitation.org/doi/10.1063/1.4974814>).

### **General rights**

Copyright for the publications made accessible via the Queen's University Belfast Research Portal is retained by the author(s) and / or other copyright owners and it is a condition of accessing these publications that users recognise and abide by the legal requirements associated with these rights.

### **Take down policy**

The Research Portal is Queen's institutional repository that provides access to Queen's research output. Every effort has been made to ensure that content in the Research Portal does not infringe any person's rights, or applicable UK laws. If you discover content in the Research Portal that you believe breaches copyright or violates any law, please contact [openaccess@qub.ac.uk](mailto:openaccess@qub.ac.uk).

## Design of a novel 5-DOF flexure-based compound alignment stage for Roll-to-Roll Printed Electronics

Weihai Chen,<sup>1</sup> Shang Yang,<sup>1, a)</sup> Jingmeng Liu,<sup>1</sup> Wenjie Chen,<sup>2</sup> and Yan Jin<sup>3</sup>

<sup>1)</sup>*School of Automation Science and Electrical Engineering, Beihang University, Beijing 100191, China*

<sup>2)</sup>*Mechatronics Group, Singapore Institute of Manufacturing Technology, Singapore*

<sup>3)</sup>*School of Mechanical and Aerospace Engineering, Queens University Belfast, UK*

(Dated: 22 November 2016)

Alignment stage is a pivotal component for Roll-to-Roll Printed Electronic (R2RPE), especially for Roll-to-Roll inkjet printing. This paper presents the design, modeling and testing of a new flexure-based compound alignment stage for R2RPE. In this design, the alignment stage has 5-DOF motions for compensating the alignment errors and only the rotation motion about the  $y$ -axis is redundant. The stage is constructed in series by four key parts and adopts a compounded flexure structure to achieve a great performance. Each part is driven by a PZT or VCM actuator to obtain one or two DOF motion. In order to enlarge the travel range of the alignment stage, a Scott-Russell mechanism and a lever mechanism are arranged in series for forming a two-grade displacement amplifier to overcome the small displacement of the actuator. Based on the pseudo-rigid-body simplification method, alignment models are developed. Kinematic and static analyses are conducted to evaluate the performance of the stage in terms of travel range and input stiffness. Finite element simulation is carried out to examine the mechanical performance and the theoretical models. A prototype is fabricated and experiments are conducted. Results show that the proposed alignment stage possesses an error compensation workspace of  $148.11\mu\text{m} \times 149.73\mu\text{m} \times 813.61\mu\text{m} \times 1.558\text{mrad} \times 3.501\text{mrad}$  with output coupling errors of 0.693% and 0.637% between the  $x$ - and  $y$ -axis, which meets the requirements of Roll-to-Roll inkjet printing.

<sup>a)</sup>Electronic mail: [ustbyangs@163.com](mailto:ustbyangs@163.com)

## INTRODUCTION

Printed Electronics is an electronics manufacturing technology, which can be used to produce Organic Light Emitting Diode (OLED), Organic Thin Film Transistor (OTFT) and Flexible Printed Sensor (FPS), and these products can be used in biomedical, military and aerospace fields<sup>1-4</sup>. Different from the common processing methods of electronic components, printed electronics has the advantages of low production cost, simple process and high efficiency. Therefore, Printed Electronics technology has unique competitiveness and broad application prospects. As well known, traditional printed electronic techniques include Relief Printing, Intaglio Printing, Planographic Printing, Screen Printing, etc.<sup>4</sup>. Compared with the aforementioned contact printing technology, inkjet printing has advantages of high resolution, less ink, low cost, and diversification of printed graphics, so inkjet printing has been widely used in printing electronics industry. Roll-to-Roll inkjet printing is a kind of rotary printing technique that allows target flexible polymer films to move constantly when the multilayer circuits are printed on it, as shown in FIG. 1<sup>4-6</sup>. For multilayer Roll-to-Roll Printed Electronic (R2RPE), the alignment error, i.e, the position and angular error between different layers as shown in FIG. 2, causes low overlayer registration accuracy, which will result in unacceptable resolution of the printed patterns<sup>7,8</sup>. Registration accuracy is generally only 40-100 $\mu\text{m}$  and the resolution of printing pattern is about 100 $\mu\text{m}$ <sup>9-11</sup>. Nevertheless, the current printing accuracy cannot meet the requirement of the high precision electronic equipment. In order to improve the registration accuracy, a precision alignment system which can compensate errors between layers is essential for high-precision printed electronic devices.

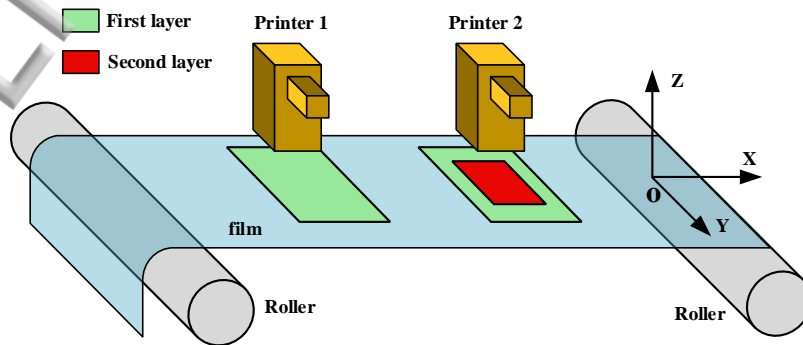


FIG. 1. Diagrammatic sketch of R2RPE.

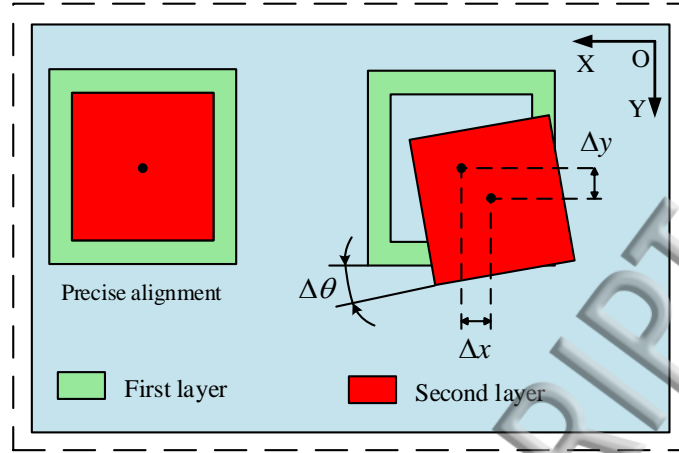


FIG. 2. Registration error of overlay alignment.

Registration error has become the biggest obstacle in improving alignment accuracy. Many scholars have done related research and achieved certain results. Professor P. R. Pagilla<sup>12,13</sup> at Oklahoma State University proposed a novel method to eliminate errors on the basis of analyzing sources of errors. The method works for compensating the error of the  $x$  Direction. Hwan Kim et al.<sup>14,15</sup> presented a new mechanism for tension control and error control and adopted CCD cameras to detect the relative errors of patterns. The most prominent feature of this device is the ability to realize decoupling control of errors. Hyunkyoo Kang et al.<sup>16,17</sup> established a mathematical model of the  $x$  and  $y$  direction errors, and integrated the errors in both directions by an equivalent model. According to the model, a feed-forward control method was presented to control the rollers to compensate the register error. Zhuang Chen et al.<sup>18</sup> presented machine vision-based alignment system of an emerging PCB inkjet printer, which achieved good experiments result. Though the above methods played a certain role for error compensation, the register accuracy can only achieve up to 40-50  $\mu\text{m}$  because of adopting the traditional rigid hinge and transmission mechanism being adopted.

As well known, flexible mechanism has been widely used in many fields for its no friction, no backlash, no wear and ease of fabrication<sup>19</sup>, such as micropositioning, micromanipulator<sup>20,21</sup>. To further improve the accuracy, researchers have started to apply flexible mechanism to design the alignment devices for multilayer R2RPE. P. Baldesi et al.<sup>22,23</sup> designed a multi-roll to roll printed electronics registering devices by applying flexible mechanism. The agency has only two DOF for compensating errors and the compliant mechanisms are actuated man-

ally through two micrometers, so it can obtain accurate motion to achieve high-precision error compensation. Jian Zhao et al.<sup>24</sup> developed a novel alignment mechanism employing orthogonal connected multi-layered flexible hinges, the alignment precision of which reached  $1.0\ \mu\text{m}$  for centering within the range of 1 mm and 1 in. for leveling within  $\pm 1^\circ$ . Xi Zhou et al.<sup>25,26</sup> developed a flexure-based R2R platform and achieved good control effect.

Based on the literature review, it is found that the existing multi-register mechanisms are imperfect in design<sup>22,26</sup>. Their methods generally employ traditional rigid hinges and drives to adjust the registration errors between layers, which means that the accuracy of compensation mechanism cannot be guaranteed. In addition, some multi-register mechanisms have used flexible mechanism for alignment, but the design of these institutions are not perfect enough to reach high precision. In these designs, the gravity of rollers and the tension force of films are interference factors which affect the accuracy of the flexible mechanism due to its low-rigidity. The errors resulted from gravity are crucial to the accuracy of the printing device but have not been addressed in existing designs. The actual errors are relative positional deviation between the film and the printer head, so errors should be compensated by adjusting the position of printer head.

To solve the aforementioned problems, this paper proposes a decoupled 5-DOF flexure-based compound alignment stage for effective errors compensation. The stage is constituted in series by four parts and adopts a compounded flexure structure. Each part realizes one or two translational or rotational motion driven by piezoelectric actuators (PZTs) or voice coil motors (VCMs). In this design, the alignment stage has 5-DOF motions for compensating the alignment errors and only the rotation about the  $y$ -axis is redundant. The alignment stage can achieve high precision registration with the designed flexible mechanism in the five dimensions and it can be used to compensate online during the production process, which improves the production efficiency and quality of printing.

The mechanical and theoretical modeling, finit element analysis and the prototype experiment of the alignment stage are presented in this paper. The remainder of this paper is organized as follows: In Section II, design consideration, mechanical structure and motion description are presented. Theoretical modeling and parameters design are conducted in Section III. FEA to verify the effectiveness of theoretical modeling is presented in Section IV. Prototype experiments and results are discussed in Section V. Finally, the conclusion is given in Section VI.

## DESIGN OF THE 5-DOF ALIGNMENT STAGE FOR R2RPE

### A. Design considerations

The printing resolution and overlay accuracy are two key evaluation indexes and critical challenges for R2RPE, and they directly affect the quality and performance of printing electronic products. The overlay accuracy mainly depends on the performance of the alignment stage. The position and angle of the printer head relative to the film is pivotal for overlay accuracy, which means that a redundant motion between their postures will decrease the overlay accuracy. The alignment of multilayer printed electronics is a planar alignment process. There are errors in three main directions, i.e., the direction of the film motion (Machine Direction, MD), perpendicular to the direction of the film motion (Cross Direction, CD) and a deflection (Rotational Direction, RD). In addition, the deflection error and the distance error between the printer head and the film also need to be compensated. Figure. 3 shows the required DOF for compensating errors between the printer head and the film. The errors can be compensated through three translation motion along the  $x$ -axis,  $y$ -axis,  $z$ -axis, a tilting motion  $\theta_x$  about the  $x$ -axis and a rotational motion  $\theta_z$  about the  $z$ -axis. The translation along the  $z$ -axis can be actuated by a VCM to adjust the distance between the printer head and the film for accommodating different characteristics and sizes of printing inks, while other motions can be actuated by PZT actuators to adjust the relative position between the printer head and the film.

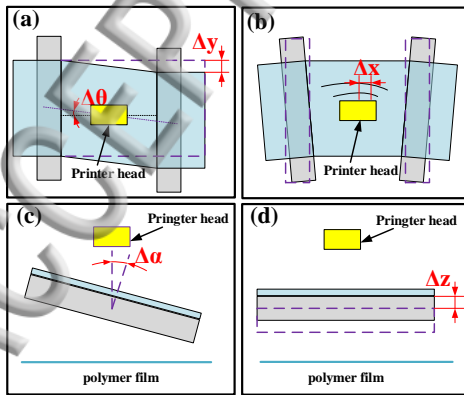


FIG. 3. The Position and angular errors.

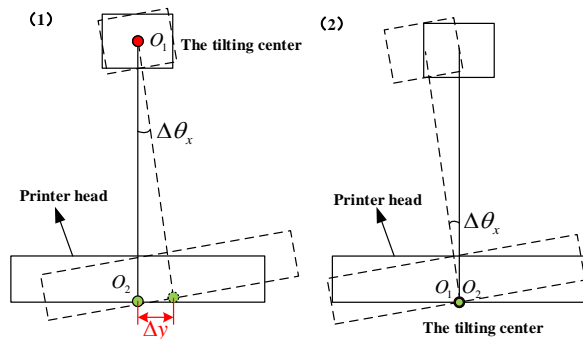


FIG. 4. The tilting motion: (a)Unreasonable center of rotation; (b)Reasonable center of rotation



Theoretically, these errors can be compensated by adjusting the printer head or the film. However, for the R2RPE equipment in this research project, in order to improve the alignment precision, gas floating roller is employed to support the film and a passive mechanism is adapted to passively adjust the tension distribution of the film. Therefore, it is inoperative for error compensation and the tension balance of film will be destroyed by adjusting the roller. Consequently, the alignment stage should be adapted to adjusting the printer head in this paper. Moreover, the tilting motions about the  $x$ -axis will bring coupling movement, thus introducing a new alignment error, as shown in FIG. 4, which is unacceptable in the alignment process. Therefore, in order to avoid this coupling movement, the tilting center of the alignment stage  $O_1$  should coincide with the center of printer head nozzle  $O_2$ , which means that the tilting center of the flexible mechanism is not within the physical boundary of the mechanism; that is to say, the flexible mechanism with the tilting motion about the  $x$ -axis should have the characteristic of Remote Center of Motion (RCM). Furthermore, to compensating errors in a larger range, the alignment stage requires large displacement strokes for achieving high accuracy. Notably, a motion cannot interfere with the other motions, so the motion decoupling should be considered.

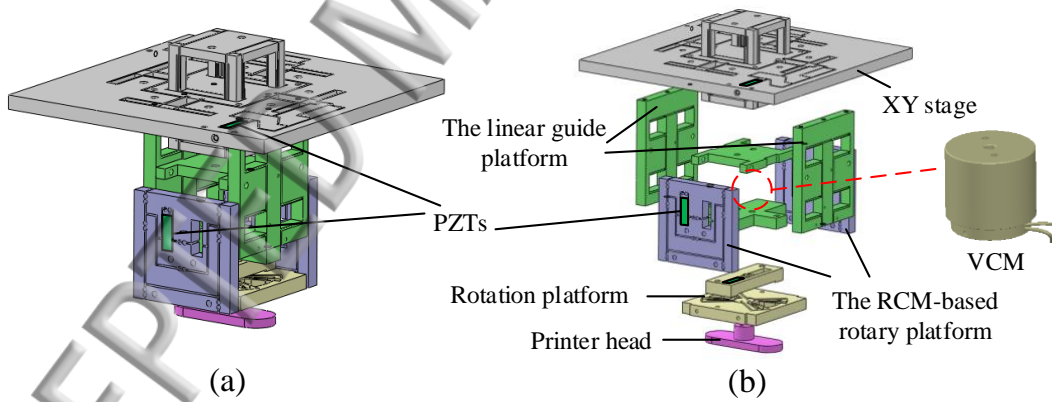


FIG. 5. The 5-DOF compound alignment stage.

## B. Mechanical structure and motion description

Based on the above analysis, a decoupled 5-DOF flexure-based alignment stage for R2RPE is proposed in this paper, as shown in FIG. 5. The alignment stage consists of four key parts in a serial manner, including an  $XY$  stage, two linear guide platforms of  $z$ -

ings, two RCM-based rotary platforms and a rotation platform about  $z$ - axis. The printer head is placed on the end of the alignment stage, so the errors can be compensated by adjusting these alignment platforms to adjust posture of the printer head. In addition, in order to reduce the assembly error and ensure the geometrical dimensions of the flexure hinges, the alignment stage is fabricated by the Wire Electrode Discharge Machining (WEDM) from the AL7075 material.

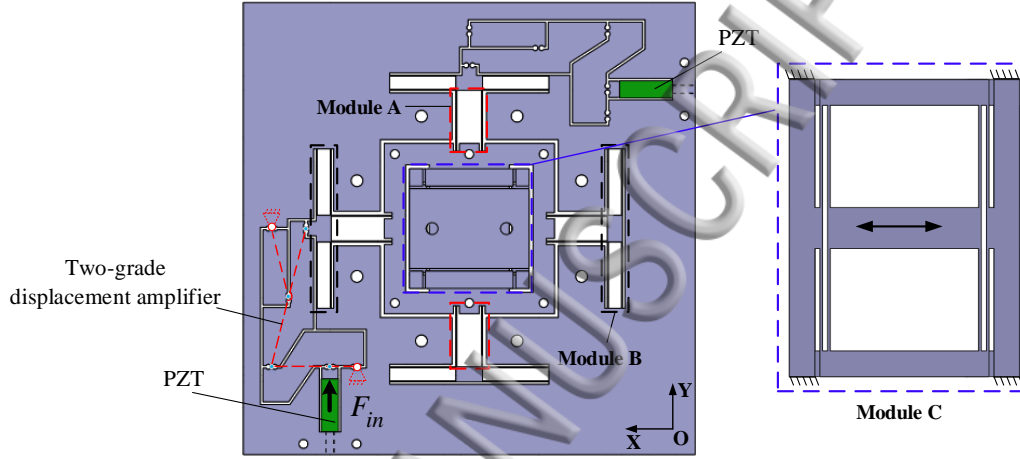


FIG. 6. The mechanism structure of XY stage.

The  $XY$  stage is a decoupled parallel 2-DOF motion platform, which is accurately controlled by two PZT actuators with two decoupled translations along the  $x$ - and  $y$ - axis respectively. In addition, the PZT actuators have characteristics of short stroke and large driving force, so a two-grade displacement amplifier, arranged in series by a Scott-Russell mechanism<sup>27</sup> and a lever mechanism, is designed to increase the output displacement of the  $XY$  stage. For the  $XY$  stage, the flexure Module A can realize the input decoupling, and a flexible parallelogram mechanism B plays a role of guiding as shown in FIG. 6. The flexible double parallelogram mechanism C is designed for output decoupling and guiding. The linear guide platform of  $z$ - axis is connected to the output of the  $XY$  stage and controlled by a VCM with a translation along the  $z$ - axis. The output plate of the linear guide platform is suspended by two identical compliant components which are designed by two compliant parallelogram mechanisms in symmetrically. This layout can minimize the parasitic motion of the output plate so as to provide a precise and smooth linear translation motion under the control of a VCM.

A typical parallelogram mechanism with a RCM is shown in FIG. 7. During the rotation



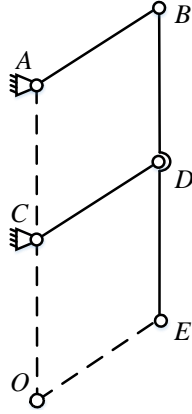


FIG. 7. Parallelogram mechanism with RCM.

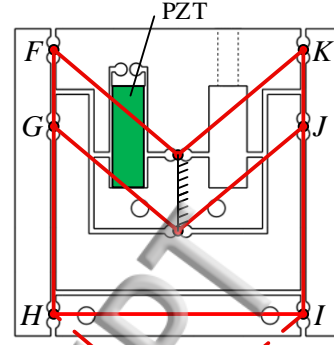


FIG. 8. The RCM-based rotary platform.

process, points  $B$  and  $C$  rotate around joints  $A$  and  $D$ , respectively, so the point  $E$  will rotate around the virtual point  $O$ . Nevertheless, a rotary positioning stage constructed with single parallelogram mechanism is unstabilized for precision alignment stage. Under the above analysis, the RCM-based rotary platform proposed in this paper is illustrated in FIG. 8, which is designed by a pair of RCM mechanism based on parallelogram mechanisms, controlled by two PZT actuators with a tilting motions  $\theta_x$  about the  $x$ -axis. The working principle of the RCM-based rotary platform is shown in FIG.8. It possesses the ability to rotate around the virtual point  $O$  without center shift and alter the initial operating space to make the tilting center of the flexible mechanism and the center of printer head nozzle coincident. The last part of the alignment stage is a rotation platform controlled by a PZT actuator as shown in FIG. 9, which is proposed to use the *butterflypivot* structure<sup>28</sup> and consists of flexible beams. In order to increase their resistance to buckling, the flexible beams have been reinforced in the middle. As mentioned above, the PZT actuator is a kind of linear displacement actuator with a short stroke and a large driving force. Therefore, within the scope of the small movement, the rotation platform should have the ability to convert the finite linear input of the PZT into a sufficient rotation output. The angle of rotation  $\varphi_{out}$  of the output induced by the input  $z_{\theta in}$  of the PZT can be expressed by:

$$\varphi_{out} = \frac{z_{\theta in}}{d_1}, \quad (1)$$

where  $d_1$  is the distance from the PZT to the center of rotation. The distance  $d_1$  decides the scope of the output angle. In order to obtain a larger output angle, the value of  $d_1$  should be small enough. Thus, a single PZT input part is employed with a small value of  $d_1$  as

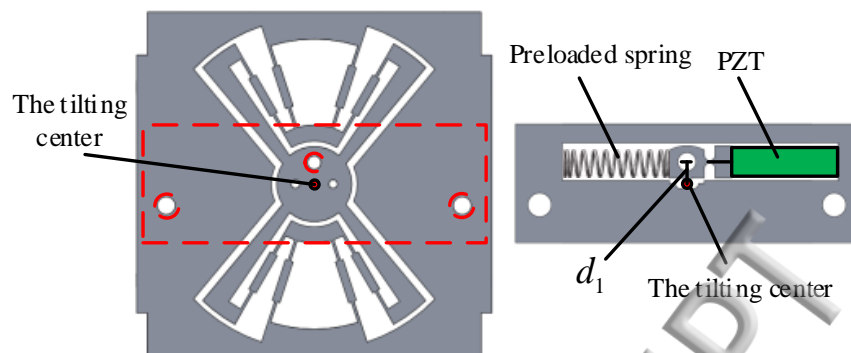


FIG. 9. The rotation platform.

shown in FIG. 9.

The proposed alignment stage and other relevant device are shown in FIG. 10. The initial errors between the printer head and the film is unavoidable on account of the manufacturing and assembly errors. In addition, the positioning precision of the motor and the mobile platform is not good enough, so the alignment stage is proposed for compensating the errors and improving the spray printing precision. During the printing process, the printer head will be moved to the printing area by the 3-axis motion platform firstly. Then, the errors will be detected the relative position of the printer head and the reserved mark of the film and sent to the control system to further drive the alignment stage to compensate errors. Hence, using the combined way of coarse positioning and accurate positioning, the alignment system can meet the requirements of wide range of jet printing and high precision alignment.

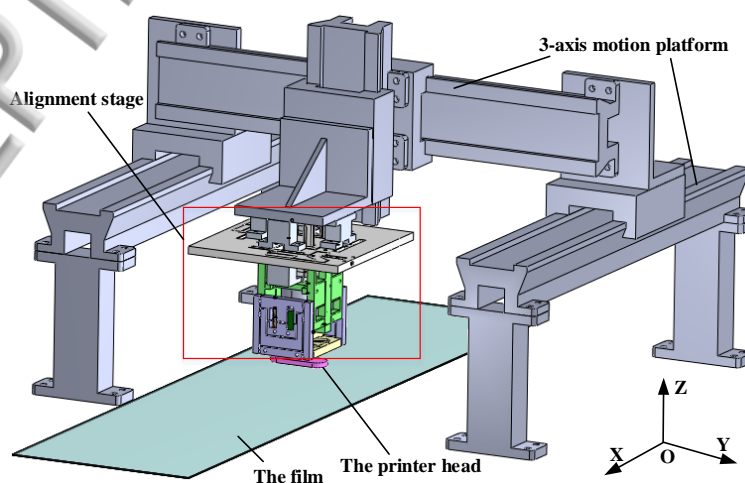


FIG. 10. The proposed alignment stage and relevant device.

## MODELING AND ANALYSIS

Based on the above analysis, the alignment stage consists of four key parts in series and each part achieve one or two DOF of movement, so we can model and calculate parameters part by part easily.

### A. Kinematic analysis

In order to analyze the kinematics of the alignment stage, the pseudo-rigid-body model (PRBM) approach is employed for its effectiveness and simplification. From the PRBM approach point of view, a flexure hinge of flexure-based mechanisms can be equivalent to an ideal single-axes revolute joint with a torsional spring<sup>29</sup>, so the drift of the rotational centers and the stiffness of flexure hinges will not be considered.

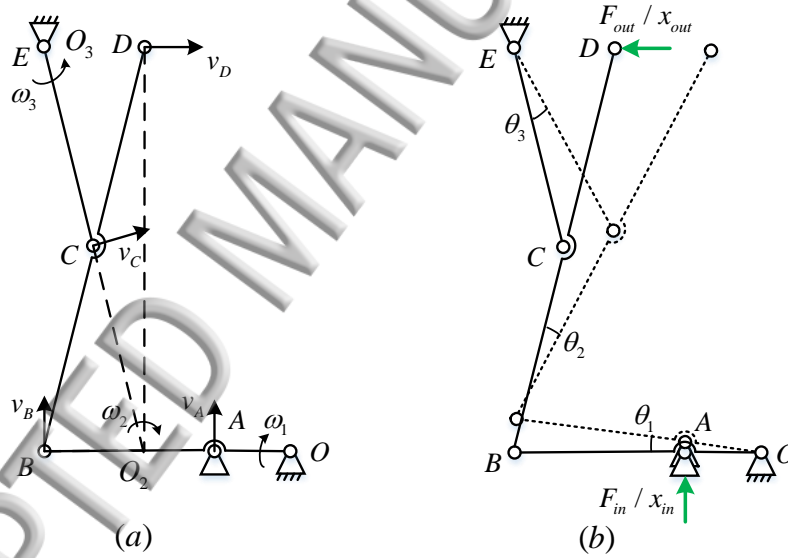


FIG. 11. Kinematic model of the displacement amplifier: (a) vector diagram; (b) displacement diagram.

For the XY stage, adapting parallel structure and the identical flexible mechanism design in  $x$  and  $y$  direction, the kinematic analysis and calculation can be conducted in one direction. The kinematic model of the displacement amplifier is shown in FIG. 11(a). As mentioned previously, the two-grade displacement amplifier is arranged in series by a Scott-Russell mechanism and a lever mechanism, and the length of linkages is identical for the Scott-Russell mechanism, i.e.,  $l_{BC} = l_{CD} = l_{CE}$ . According to the kinematic model, the theoretical

displacement amplification ratio  $R_{amp}$  can be expressed as:

$$R_{amp} = \frac{x_{out}}{x_{in}}, \quad (2)$$

where  $x_{in}$  and  $x_{out}$  represent the input and output displacements of the  $XY$  stage, respectively. In addition, based on the theory of mechanics, the instantaneous centers of the linkages can be shown in FIG. 11(a). Therefore, the instantaneous velocities of the points  $A, B, C$  and  $D$  can be calculated as:

$$v_A = \omega_1 \cdot l_{OA}, \quad (3)$$

$$v_B = \omega_1 \cdot l_{OB} = \omega_2 \cdot l_{O_2B} = \omega_2 \cdot l_{DE}, \quad (4)$$

$$v_C = \omega_2 \cdot l_{O_2C} = \omega_3 \cdot l_{CE}, \quad (5)$$

$$v_D = \omega_2 \cdot l_{O_2D} = \omega_2 \cdot l_{BE}, \quad (6)$$

where  $\omega_1$ ,  $\omega_2$  and  $\omega_3$  are the instantaneous angular velocities of the linkages  $OB$ ,  $BD$  and  $EC$ , respectively. Thus, the displacement amplification ratio can be rewritten as:

$$R_{amp} = \frac{x_{out}}{x_{in}} \cong \frac{v_D}{v_A} = \frac{l_{OB} \cdot l_{BE}}{l_{OA} \cdot l_{DE}}. \quad (7)$$

From EQ. (7), the relationship between output and input displacement of  $XY$  stage is linear and constant only dependent on the geometrical parameters of the linkages. Furthermore, the rotational angles  $\varphi_O, \varphi_A, \varphi_B \sim \varphi_E$  of the flexure hinges  $O, A, B \sim E$  are shown in FIG. 11(b), which can be written as:

$$\varphi_O = \varphi_A = \theta_1 = -\frac{x_{in}}{l_{OA}}, \quad (8)$$

$$\varphi_B = \theta_2 - \theta_1 = \frac{x_{in}}{l_{OA}} - \frac{x_{in} \cdot l_{OB}}{l_{OA} \cdot l_{DE}}, \quad (9)$$

$$\varphi_C = \theta_3 - \theta_2 = \frac{x_{in} \cdot l_{OB}}{l_{OA} \cdot l_{DE}} + \frac{x_{in} \cdot l_{OB}}{l_{OA} \cdot l_{DE}}, \quad (10)$$

$$\varphi_D = \theta_2 = -\frac{x_{in} \cdot l_{OB}}{l_{OA} \cdot l_{DE}}, \quad (11)$$

$$\varphi_E = \theta_3 = \frac{x_{in} \cdot l_{OB}}{l_{OA} \cdot l_{DE}}, \quad (12)$$

where  $l_{OA}$ ,  $l_{OB}$ ,  $l_{DE}$  are the lengths of linkages  $OA$ ,  $OB$ ,  $DE$  respectively and  $l_{OB} > l_{DE}$ , so the rotational angle  $\varphi_C$  is the maximum angle in the flexure hinges.

For the linear guide platform along the  $z$ - axis, there is no displacement amplifier and the compliant parallelogram mechanism plays a role of guidance and positioning, so the output and input are equal theoretically, which can be written as:

$$z_{out} = z_{in}, \quad (13)$$

where  $z_{in}$  and  $z_{out}$  represent the input displacement of VCM and the output displacement of the platform, respectively.

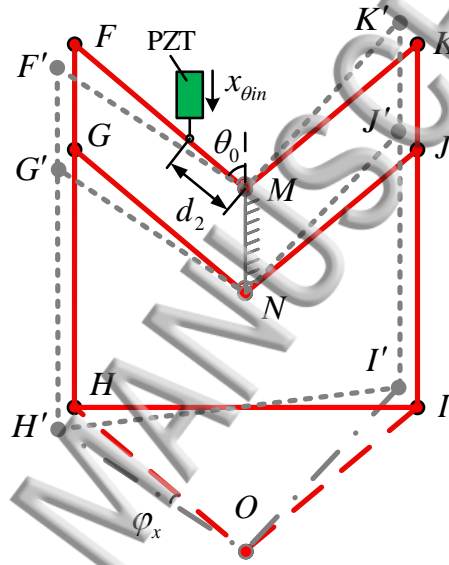


FIG. 12. The kinematic model diagram of the RCM-based rotary platform.

The RCM-based rotary platform transforms the displacement input of the PZT on a tilting angle about the  $x$ - axis and the kinematic displacement diagram is shown as FIG. 12. The RCM-based rotary platform will move to a new position with a displacement  $x_{\theta in}$  driven by the PZT actuator. According to the characteristics of the parallelogram mechanism, these flexure hinges will rotate with an identical angle, which can be expressed by:

$$\varphi_x = \theta_{in} = \frac{x_{\theta in}}{d_2 \cdot \sin \theta_0}, \quad (14)$$

where  $\theta_0$  and  $d_2$  are the original input angle and the length between the input point and the rotation center  $M$ , respectively. Due to the geometric relationship, the output rotation angle can be calculated by:

$$\theta_{out} = \theta_{in}. \quad (15)$$

For the rotation platform about  $z$ -axis, the output rotation angle and input displacement has be calculated by EQ. (1) and the rotational angle  $\varphi_z$  is given as:

$$\varphi_z = \frac{z_{\theta in}}{d_1}. \quad (16)$$

## B. Stiffness modeling

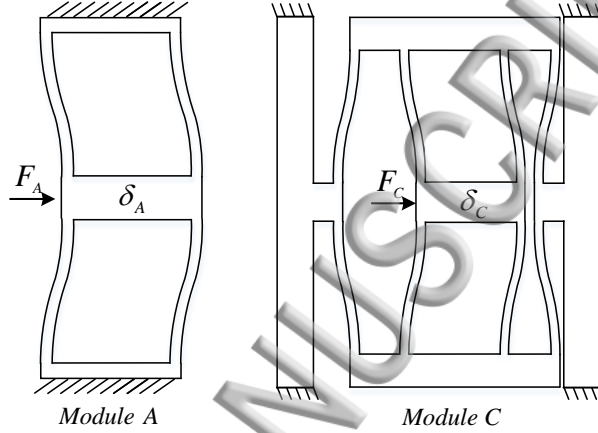


FIG. 13. The deformation of module  $A$  and  $C$  under external force.

The stiffness is an important indicator for the determination of actuators and geometrical parameters. According to the above analysis, the stiffness can be calculated on the different degrees of freedom, individually. The constituent flexure elements of the  $XY$  stage without the amplifier are two kind of flexure modules, and the deformations of module  $A$  and  $C$  under external force are shown in FIG. 13. The deformation behavior of a flexure beam is shown as FIG. 14. Given the boundary condition of the zero rotation angle at the free end, the equations can be described as:

$$M = \frac{Fl}{2}, \quad (17)$$

$$\delta = \frac{Fl^3}{12EI}, \quad (18)$$

where  $\delta$  is the transverse displacement at the free end,  $E$  is the elastic modulus of the material,  $I = bt^3/12$  denotes the moment of inertia of the cross section and  $l$ ,  $b$ ,  $t$  represent the length, width and thickness of the flexure beam as shown in FIG. 14. Then, the stiffness of the flexure modules  $A$ ,  $B$  at the output direction can be derived as:

$$K_A = \frac{F_A}{\delta_A} = \frac{4F}{\delta} = \frac{4Ebt_1^3}{l_1^3}, \quad (19)$$



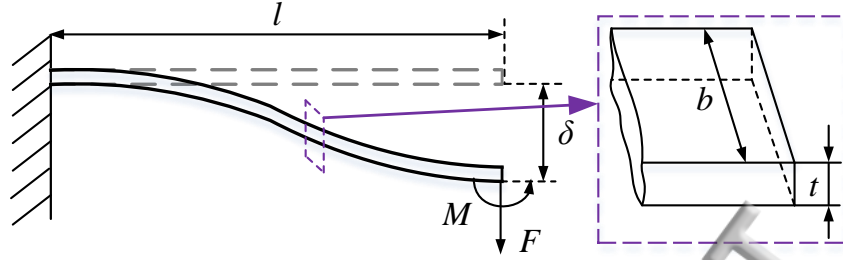


FIG. 14. The force analysis of a flexure beam.

$$K_B = \frac{F_B}{\delta_B} = \frac{4F}{\delta} = \frac{4Ebt_2^3}{l_2^3} \quad (20)$$

$$K_C = \frac{F_C}{\delta_C} = \frac{4F}{2\delta} = \frac{2Ebt_3^3}{l_3^3} \quad (21)$$

Then, the stiffness of the XY stage without the amplifier can be obtained as follows:

$$K_{x1} = K_A + 2K_B + 2K_C = \frac{4Ebt_1^3}{l_1^3} + \frac{8Ebt_2^3}{l_2^3} + \frac{4Ebt_3^3}{l_3^3} \quad (22)$$

Similarly, for the linear guide platform along the z-axis, the flexible element is the flexible beam, so the stiffness can be obtained as:

$$K_z = \frac{F_{zin}}{Z_{in}} = \frac{F_{zin}}{Z_{out}} = \frac{8Ebt_4^3}{l_4^3} \quad (23)$$

For the XY stage, the stiffness of XY stage without the amplifier has been calculated individually, which will be taken when the external force  $F_{out}$  is applied in the output end point of amplifier, so the following equation can be obtained.

$$F_{out} = K_{x1} \cdot x_{out} = K_{x1} \cdot R_{amp} \cdot x_{in} \quad (24)$$

The PRBM of the amplifier is shown in FIG. 11(b). According to the above analysis, the rotational angles of all the flexure hinges have been calculated when the input force applied at the input point. For circular flexure hinge, the rotational stiffness can be estimated and expressed as<sup>30</sup>:

$$K_r = \frac{2Ebh^{5/2}}{9\pi r^{1/2}} \quad (25)$$

Given that the input force  $F_{in}$  from the PZT actuator is applied to the input end with the input displacement, the input force work  $W_1$  can be expressed as:

$$W_1 = \frac{1}{2} F_{xin} \cdot x_{in} \quad (26)$$

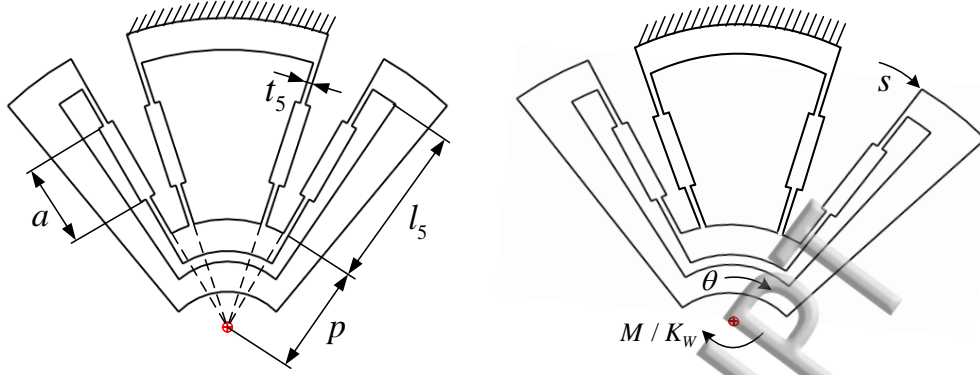


FIG. 15. Schematic of the rotation platform about  $z$ - axes: (a) flexure beams, (b) reinforced beams.

According to the conservation of energy, the input force work  $W_1$  is transformed into elastic potential energy and used to overcome the external force. So the following equation can be developed:

$$W_1 = E_1 = \sum_{i=A}^E \frac{1}{2} k_r \varphi_i^2 + \frac{1}{2} k_r \varphi_O^2 + \frac{1}{2} F_{out} x_{out}. \quad (27)$$

According to the EQ. (8)-(12), the following equation is obtained:

$$K_x = \frac{F_{xin}}{x_{in}} = \frac{K_r}{l_{OA}^2} \cdot \left( \frac{7l_{OB}^2}{l_{DE}^2} - \frac{2l_{OB}}{l_{DE}} + 3 \right) + K_{x1} \cdot R_{amp}^2, \quad (28)$$

where  $K_x$  is the input stiffness of the alignment stage along the  $x$ - axis. Due to the symmetrical property, the stiffness along  $x$ - and  $y$ - axis are equal:

$$K_y = K_x. \quad (29)$$

Similarly, the PRB model of the RCM-based rotary platform is shown as FIG. 12. The rotational angles of all the flexure hinges have been calculated when the input force  $F_{\theta xin}$  applied at the input point. According to the conservation of energy, the following equation can be developed:

$$W_2 = \frac{1}{2} F_{\theta xin} x_{\theta in} = E_2 = 9 \cdot \frac{1}{2} k_r \varphi_x^2. \quad (30)$$

Then, the input stiffness  $K_{\theta x}$  of the alignment stage of the alignment stage about the  $x$ -axis can be obtained as:

$$K_{\theta x} = \frac{F_{\theta xin}}{x_{\theta in}} = \frac{9K_r}{d_1^2 \cdot \sin^2 \theta_0}. \quad (31)$$

For the rotation platform about the  $z$ -axis, as show in FIG. 15, the rotational stiffness can be calculated<sup>31</sup>:

$$K_W = EI \frac{a^2 + al_5 + 4(l_5^2 + 3l_5p + 3p^2)}{(l_5 - a)(a^2 + al_5 + l_5^2)}. \quad (32)$$

According to the conservation of energy, the following equation can be developed:

$$W_3 = \frac{1}{2} F_{\theta_{zin}} z_{\theta_{in}} = E_2 = \frac{1}{2} k_r \varphi_z^2 + \frac{1}{2} \cdot 2k_w \varphi_z^2, \quad (33)$$

where  $F_{\theta_{zin}}$  represents the input force and  $z_{\theta_{in}}$  represents the input displacement. According to EQ. (2), the input stiffness  $K_{\theta_z}$  of the alignment stage about  $z$ -axis can be obtained as:

$$K_{\theta_z} = \frac{F_{\theta_{zin}}}{z_{\theta_{in}}} = \frac{K_r + 2K_w}{d_1^2}. \quad (34)$$

### C. Critical load of buckling

As the  $XY$  stage is constructed by a series of slender flexure beams, it suffers from the axial load during operations. Buckling, which impacts the instability of the structure, should be avoided. For a flexure beam, the critical load can be calculated by:

$$P_{cr} = \frac{\pi^2 EI}{l_{cr}^2}, \quad (35)$$

where  $I = bt^3/12$  is the area moment of inertia of the cross section, and  $l_{cr}$  represents the critical length, which can be decided by:

$$l_{cr} = \mu l, \quad (36)$$

where the coefficient  $\mu$  depends on the boundary conditions. For the flexure beam with the two fixed ends in the  $XY$  stage, the value of  $\mu$  is 0.5<sup>32</sup>. According to the structure of the  $XY$  stage, the critical load  $F_{cr}$  can be calculated as:

$$F_{cr} = 2P_{cr} = \frac{8\pi^2 EI}{l^2}. \quad (37)$$

In order to avoid the elastic buckling deformation of the slender flexure beams, the axial load on the slender flexure beams should satisfy:

$$F_{out} \leq F_{cr}. \quad (38)$$

Hence, the stiffness of  $XY$  stage without the amplifier should be met:

$$K_{x1} = \frac{8Eb_A t_A^3}{l_A^3} + \frac{4Eb_B t_B^3}{l_B^3} + \frac{4Eb_C t_C^3}{l_C^3} \leq \frac{F_{cr}}{R_{amp} x_{in}} = \frac{8\pi^2 EI}{R_{amp} x_{in} l^2}. \quad (39)$$

The parameters of flexible mechanisms should satisfy the above condition in order to avoid the elastic buckling deformation.

TABLE I. Parameters of material and flexure-beams

Parts of alignment stage	Parameters	Description	Value( $mm^3$ )
XY stage	$l_1 \times t_1 \times b$	Dimensions of flexure module A	$23 \times 0.3 \times 8$
	$l_2 \times t_2 \times b$	Dimensions of flexure module A	$25 \times 0.3 \times 8$
	$l_3 \times t_2 \times b$	Dimensions of flexure module B	$20 \times 0.5 \times 5$
	$r_1 \times h_1 \times b$	Dimensions of flexure joint	$1 \times 0.4 \times 8$
Linear guide platform	$l_4 \times t_4 \times b$	Dimensions of flexure joint	$21 \times 0.4 \times 8$
RCM-based rotary platform	$r_2 \times h_2 \times b$	Dimensions of flexure joint	$1.25 \times 0.5 \times 8$
Rotation platform	$r_3 \times h_3 \times b$	Dimensions of flexure joint	$1 \times 0.4 \times 8$
	$l_5 \times t_5 \times a \times b$	Dimensions of flexure beam	$16 \times 0.5 \times 8 \times 8$
$d_1$	$\theta_0$	$d_1$	p
4mm	$50^\circ$	12.75mm	11mm
Density ( $\rho$ )	Young's modulus ( $E$ )	Tensile strength( $\sigma_b$ )	Poisson ratio ( $\nu$ )
2810 kg/m <sup>3</sup>	71.7Gp	503Mp	0.33

#### D. Parameters design

For the alignment stage, motion range and stiffness are the two main factors to determine the performance of the alignment stage, which mainly depends on the geometrical parameters of flexible elements. So the geometrical and material parameters should be determined on the basis of the design requirements. For printer head, a wide range of movement will be conducted by the XYZ linear motion platform, and the small stroke movement with high precision will be conducted by the alignment stage. According to the requirements of error compensation, using the combined way of coarse positioning and accurate positioning, the alignment stage adjusting range  $x \times y \times z \times \theta_x \times \theta_z$  should be  $120\mu m \times 120\mu m \times 800\mu m \times 1.5mrad \times 3.5mrad$ . Therefore, the final geometrical and material parameters are determined as listed in Table I.

## FINITE ELEMENT ANALYSIS

In order to verify the performance of the alignment stage, finite element simulation is conducted with the software ANSYS Workbench 14.5. The values of material and structure parameters are listed in TABLE I. The deformation, stress distribution and stiffness of each part of the alignment stage will be discussed in this section, respectively.

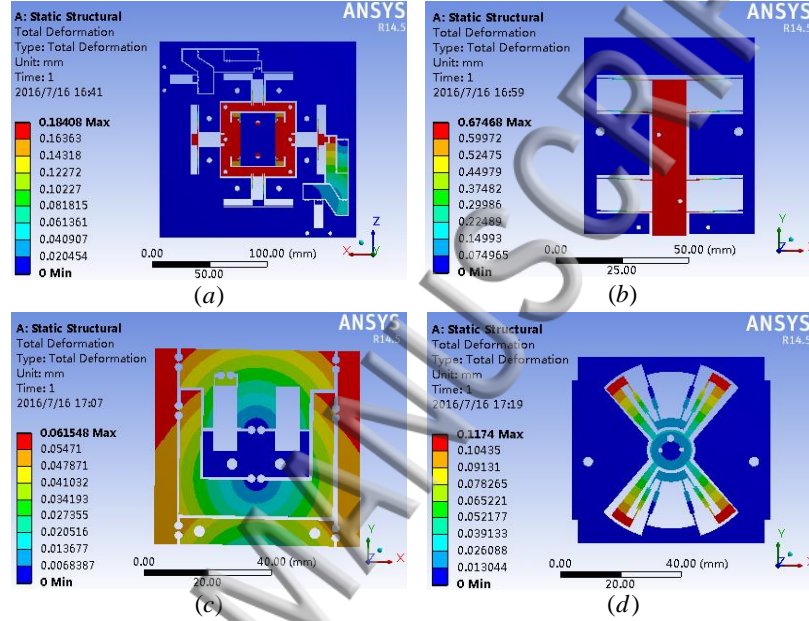


FIG. 16. Deformation simulations of the four key parts of the alignment stage: (a)  $x$  or  $y$  direction (input displacement 17.4  $\mu\text{m}$ ), (b)  $z$  direction (input displacement 500  $\mu\text{m}$ ), (c)  $\theta_x$  direction (input displacement 17.4  $\mu\text{m}$ ), (d)  $\theta_z$  direction (input displacement 17.4  $\mu\text{m}$ ).

With the maximum displacements (17.4  $\mu\text{m}$  for PZT) or maximum continuous input force (22.6 N for VCM) applied at the input end of each part of the alignment stage, the total deformation of each part is shown in FIG. 16. It can be seen that the output movement complies with the design requirement, which verifies the effectiveness of the designed alignment stage. Besides, the maximum output displacements or tilting angle can be obtained. For the XY stage, the maximum output displacement in  $x$ - or  $y$ - axis under the maximum input displacements (17.4  $\mu\text{m}$ , the stroke of the PZT) is 184.08  $\mu\text{m}$ . For Linear guide platform, the maximum output displacement in  $z$ - axis under the maximum input force (22.6N, the maximum continuous force of the VCM) is 674.68  $\mu\text{m}$ . Similarly, the maximum output tilting angles about  $x$ - and  $z$ - axis under the maximum input displacements (17.4  $\mu\text{m}$ ) are



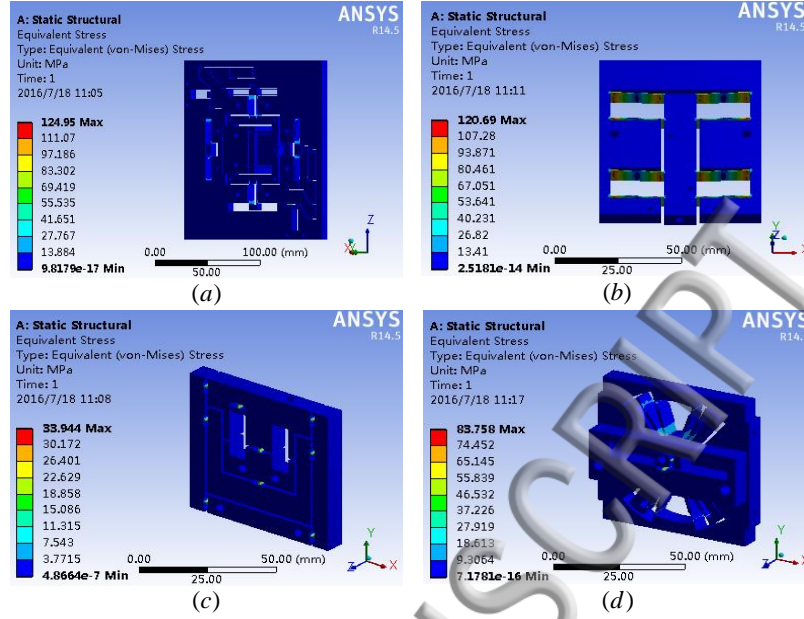


FIG. 17. Stress distribution of the four parts of alignment stage: (a) XY stage (input displacement  $17.4 \mu\text{m}$ ), (b) Linear guide platform (input displacement  $500 \mu\text{m}$ ), (c) RCM-based rotary platform (input displacement  $17.4 \mu\text{m}$ ), (d) Rotation platform (input displacement  $17.4 \mu\text{m}$ ) .

$1.753 \text{ mrad}$  and  $4.065 \text{ mrad}$ , respectively. Furthermore, the stress distributions of each part are illustrated in FIG. 17. It is found that the stress concentration only occurs at flexure hinges, and the maximum stress is  $124.95 \text{ MPa}$ , which is far lower than the yield strength of the material ( $503 \text{ MPa}$ ), so the parameters design of the alignment stage is reasonable.

For calculating the stiffness of the alignment stage, a set of forces will be exerted at the input end of each part. With a group of input displacements from  $2 \mu\text{m}$  to  $20 \mu\text{m}$  applied at the input end, the curves about force-input displacement and output-input displacement are plotted in FIG. 18(a), which provide the displacement amplification ratio and the stiffness of the XY stage. It can be observed that the input stiffness in  $x$ - or  $y$ - axis is  $5.96 \text{ N}/\mu\text{m}$ . Due to the effect of resistance from the Scott-Russell and parallelogram mechanisms, the actual displacement amplification ratio is approximately 10.51, smaller than the theoretical amplification ratio 12.8. For the Linear guide platform, with a group of input displacements from  $50 \mu\text{m}$  to  $500 \mu\text{m}$  applied at the input end, the curves about force-input displacement and output-input displacement are plotted in FIG. 18(b). According to the curves, the input stiffness is  $0.0351 \text{ N}/\mu\text{m}$ . Similarly, with a group of input displacements from  $2 \mu\text{m}$  to  $20 \mu\text{m}$  applied at the input end of the RCM-based rotary platform and Rotation platform



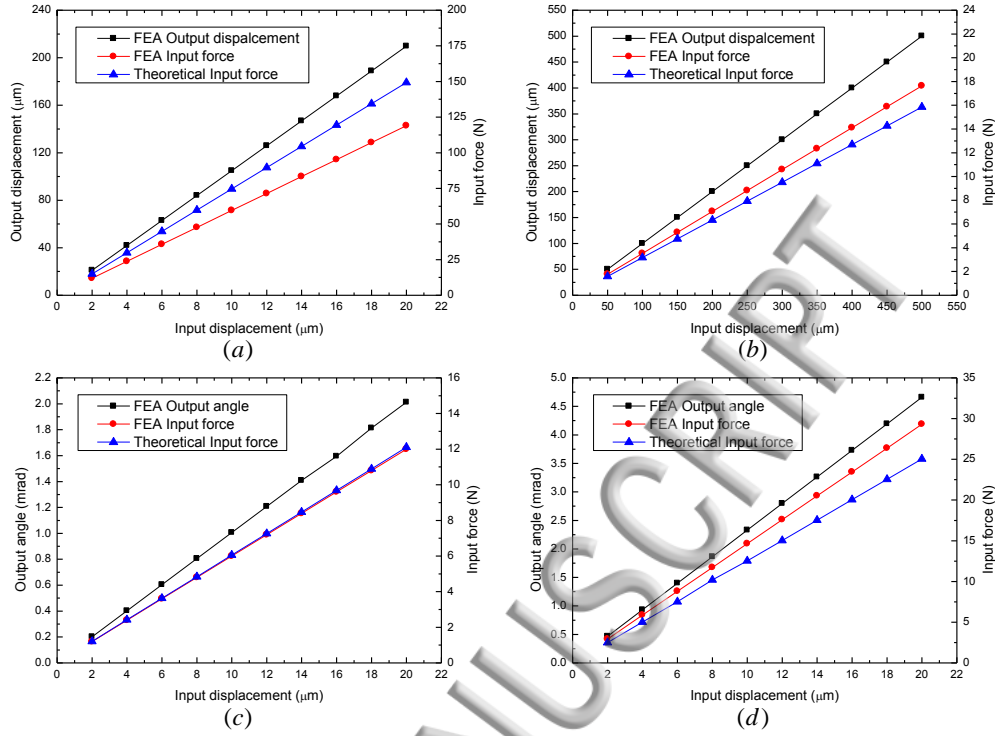


FIG. 18. Relationships of input force, input displacement and Output displacement or angle of the stage: (a)  $x$  or  $y$  direction, (b)  $z$  direction (c)  $\theta_x$  direction, (d)  $\theta_z$  direction .

of  $z$ - axis, the relationships of force-input displacement and output-input displacement are plotted in FIG. 18(c) and FIG. 18(d), respectively. It can be observed that the input stiffness are  $0.60524 \text{ N}/\mu\text{m}$  and  $1.4651 \text{ N}/\mu\text{m}$  respectively. The FEA input stiffness and the corresponding theoretical input stiffness of the alignment stage are listed in Table II. It can be seen that there is a small discrepancy between the theoretical results and FEA results. This difference is acceptable in consideration of the nonlinear characteristics of the flexure elements.

TABLE II. Parameters of material and flexure-beams

Parameters	Description	Unit	Model	FEA
$K_x$ or $K_y$	Input stiffness in $x$ - or $y$ - axis	$\text{N}/\mu\text{m}$	7.45	5.96
$K_z$	Input stiffness in $z$ - axis	$\text{N}/\mu\text{m}$	0.0317	0.0351
$K_{\theta_x}$	Input stiffness about $x$ - axis	$\text{N}/\mu\text{m}$	0.5998	0.6052
$K_{\theta_z}$	Input stiffness about $z$ - axis	$\text{N}/\mu\text{m}$	1.2527	1.4651

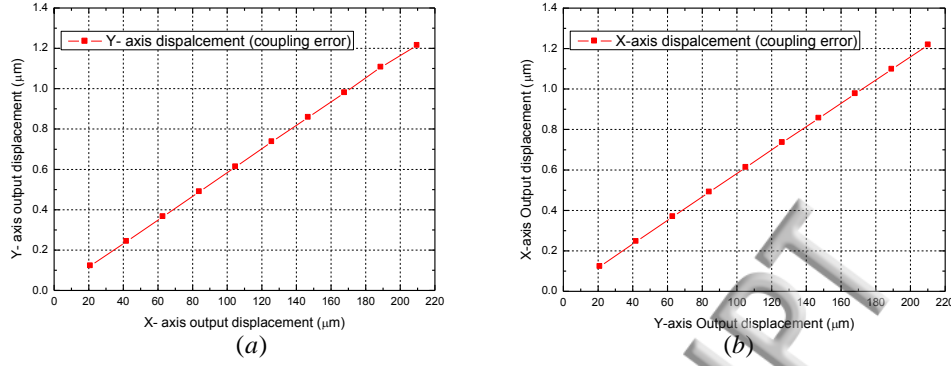


FIG. 19. The cross-coupling error analysed by FEA: (a) Y- axis coupling error, (a) X- axis coupling error.

Besides, to verify the motion precision, the cross-coupling error between the two axis is analyzed as shown in FIG. 19. Simulation results indicate that the maximum cross-coupling error is less than  $1.218 \mu\text{m}$  under the output displacement  $210.30 \mu\text{m}$ , and the cross-coupling error between the two axes is about  $0.58\%$ , which further confirms that the XY stage possesses a good decoupling performance.

## V. EXPERIMENTAL DEMONSTRATION

To investigate the performance of the alignment stage design, a prototype is fabricated by the WEDM technique with AL7075-T651 material. Five piezoelectric stack actuators with a voltage of  $0\text{--}150 \text{ V}$  (AE0505D16F, produced by Thorlabs, Inc.) are selected to drive the alignment stage. Their nominal stroke and blocking force are  $17.4 \pm 2.0 \mu\text{m}$  and  $861.8 \text{ N}$ , respectively. Considering the restrictions of the structure, the PZTs are installed in the XY stage with appropriate pre-tightening by tightening the screw and the rest PZTs are pre-tighten by preloaded springs. In addition, a voice coil motor (XVLC80-06-00A, produced by Onesworks, Inc.) is adopted to drive the linear guide platform along  $z$ - axis. Its nominal stroke, peak force and continuous force are  $6.3 \text{ mm}$ ,  $80 \text{ N}$  and  $22.6 \text{ N}$  respectively. According to the experimental setup, the input displacement, output displacement and the cross-coupling error are measured by two capacitive sensors (CPL190, probe model: C8-2.0-2.0, from Lion Precision, Inc.) with a resolution of  $4 \text{ nm}$ , a measuring range of  $250 \mu\text{m}$  and linearity better than  $0.10\%$ . Due to the requirement of a larger measurement range, the input displacement and output displacement along  $z$ - axis are measured by the MicroE II

4800 linear encoder (Mercury II 4800, produced by MicroE Systems Inc.) and high-accuracy laser displacement sensor (LK-H020, produced by KEYENCE, Inc.). The alignment stage is supported by a metal frame and placed in a vibration-isolated optical platform. The experimental setup of the alignment stage is shown in FIG. 20.

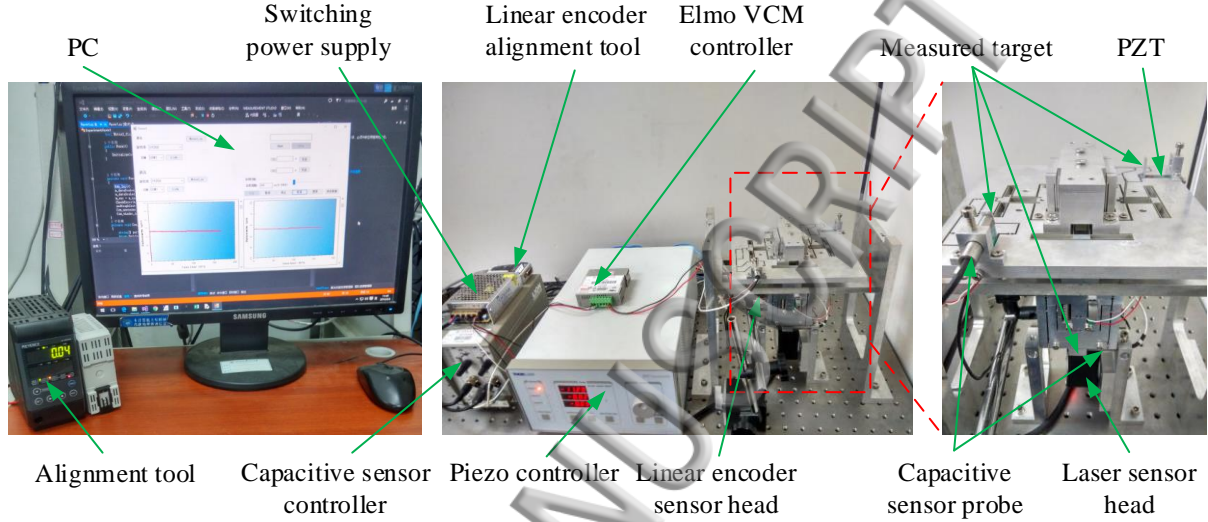


FIG. 20. Experimental setup of the alignment stage for performance tests.

First, the relationships between input displacement and output displacement/angle are tested, and the experiments are carried out under the open-loop control. When the alignment stage is driven by PZTs to translate along the  $x$ - and  $y$ - axis, the mobile platform displacement in the corresponding direction is measured by the capacitive sensor. The experimental results for the motion test along the two axis are shown as FIG.21 (a), (b). It is

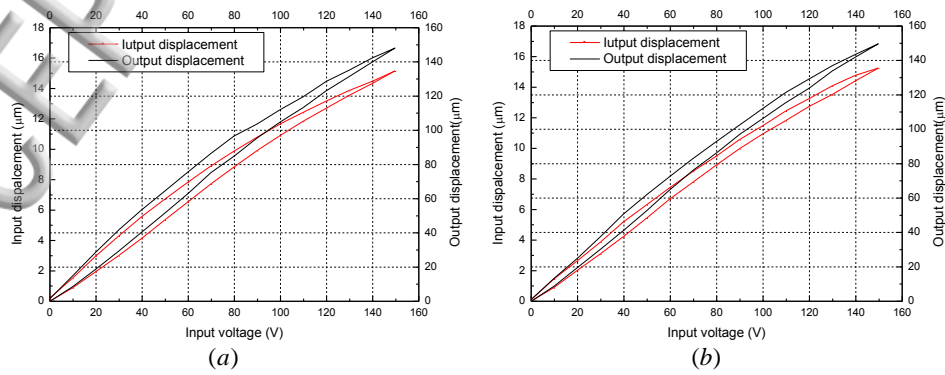


FIG. 21. Experimental results of input voltage versus input and output displacements, (a)  $x$ - axis, (b)  $y$ - axis.

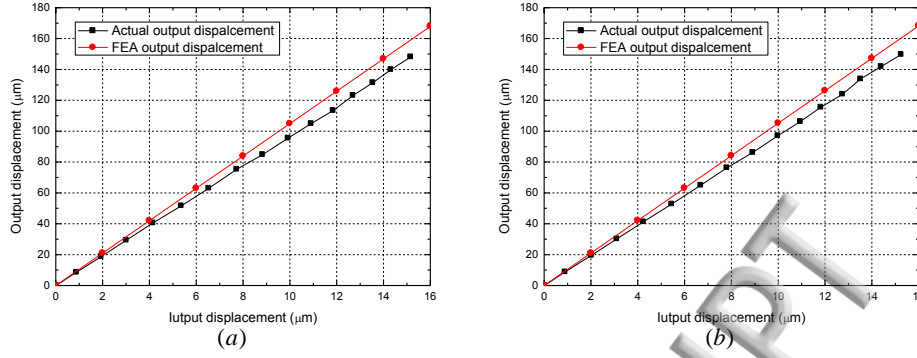


FIG. 22. Experimental results of input displacement-output displacement relationship, (a)  $x$ - axis, (b)  $y$ - axis.

observed that the maximum displacements of the PZT actuators are  $15.163 \mu\text{m}$  and  $15.256 \mu\text{m}$  along the  $x$ - axis and  $y$ - axis respectively, which are less than their nominal strokes due to the effects of the flexure hinges stiffness. In addition, the hysteresis behaviors can be seen from the curves, which is the inherent nonlinear characteristic of the PZT actuators. According to the FIG. 22 (a), (b), the output and input displacements remain linear relationship and the output displacements along  $x$ - and  $y$ - axis are  $148.11 \mu\text{m}$  and  $149.73 \mu\text{m}$  under the actual input displacements  $15.163 \mu\text{m}$  and  $15.256 \mu\text{m}$  respectively. These are smaller than the simulation results  $184.08 \mu\text{m}$  and  $184.50 \mu\text{m}$  predicted by FEA under the theoretical input displacement  $17.4 \mu\text{m}$ . The difference is mainly attributed to the effect of the stiffness of flexure elements and the preloaded forces. Besides, the experimental results along  $z$ - axis is shown in FIG. 23. It can be seen that the output and input displacement remain a linear relationship in  $z$ - axis and the output displacements along the  $z$ - axis are  $375.85 \mu\text{m}$  and  $-437.76 \mu\text{m}$ , which are less than the simulation results. The deviation is mainly attributed to the loss of VCM under the effect of the stiffness of flexure elements.

For the two rotational DOFs, the measurement of component values of the rotational angles ( $\Delta\theta_x$  or  $\Delta\theta_z$ ) is shown in FIG. 24 and it can be separately calculated by

$$\Delta\theta_x = \frac{\delta_x}{l_x}, \quad (40)$$

and

$$\Delta\theta_z = \frac{\delta_z}{l_z}, \quad (41)$$

where  $l_x = 37.5 \text{ mm}$  and  $l_z = 25 \text{ mm}$ . The values of  $\delta_x$  and  $\delta_z$  can be measured by these capacitive sensors, so the rotational angles can be calculated by EQ. (40)-(41). The experi-

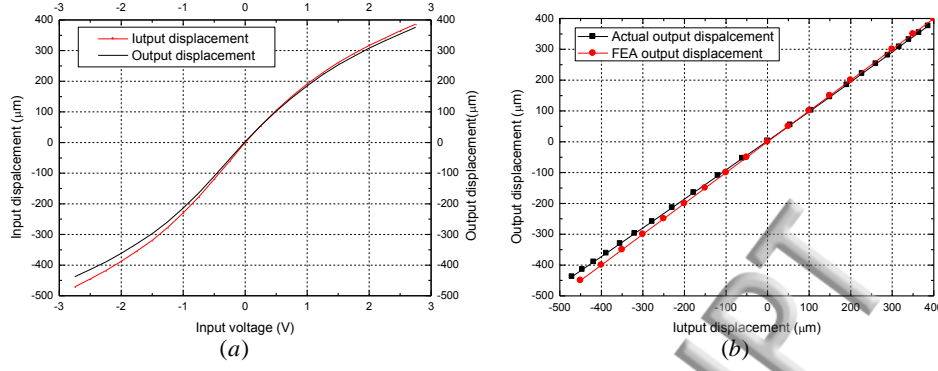


FIG. 23. Experimental results in  $z$ -axis, (a) relationship of input voltage, input displacement and output displacement, (b) input displacement-output displacement relationship.

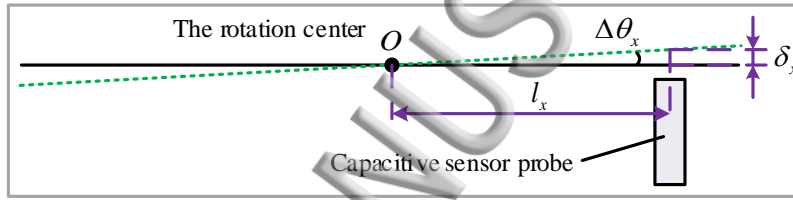


FIG. 24. Schematic diagram for measuring the rotational angle.

Experimental results of input displacement and output angle against the input voltage are shown in FIG. 25(a) and (b). It can be noticed that the maximum output angles about  $x$ -axis and  $z$ -axis are 1.558 mrad (actual input displacement 16.483  $\mu\text{m}$ ) and 3.501 mrad (actual input displacement 16.539  $\mu\text{m}$ ) respectively, while the FEA results about  $x$ - and  $z$ -axis are 1.753 mrad and 4.065 mrad respectively under the theoretical maximum input displacement 17.4  $\mu\text{m}$ . The deviation of this test from the FEA results may arise from the manufacturing tolerances of the alignment stage and the displacement loss of PZTs. However, the output angle and input displacement remain linear relationships about  $x$ - and  $z$ -axis respectively, as shown in FIG. 26.

Second, the output coupling errors of the alignment stage are tested. As previously stated, the alignment stage is constituted in series by four key parts and the  $XY$  stage is a 2-DOF parallel micropositioning stage. Therefore, the output coupling errors in  $x$  and  $y$  directions should be considered. When the stage is driven to translate along the  $x(y)$ -direction, the mobile platform displacement (output coupling error) along  $y(x)$ -axis is measured by the capacitive sensor to determine the coupling errors along the two axis. The



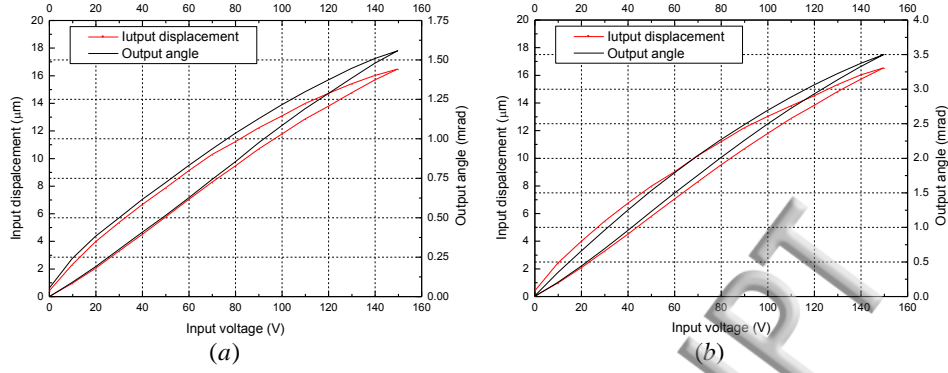


FIG. 25. Experimental results of input voltage-input displacement and output angle relationship, (a) $\theta_x$ - direction, (b) $\theta_z$ - direction.

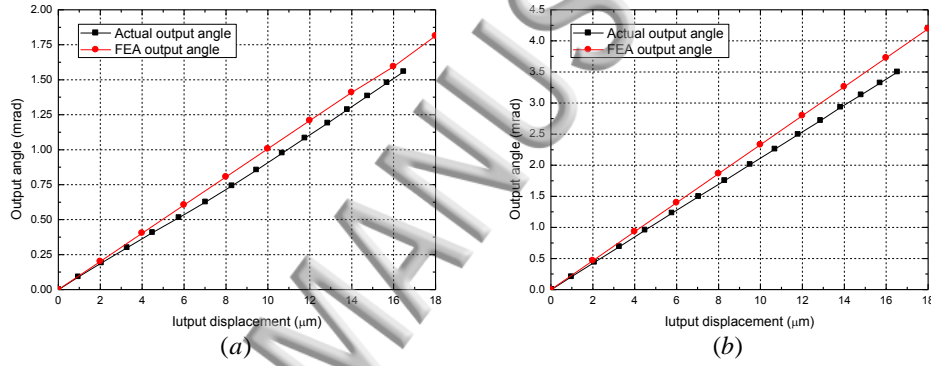


FIG. 26. Experimental results of the relationships between input displacement and output angle, (a) $\theta_x$ - direction, (b) $\theta_z$ - direction.

experimental results for the coupling errors test along the two axes are shown in FIG. 27. It is observed that the maximum crosstalk of 0.693% and 0.637% between the two working axes, larger than the FEA result (0.58%). The deviation may arise from the manufacturing tolerances of the stage and the error of capacitive sensors. The experimental results indicate that the alignment stage possesses a good decoupling performance.

In the future work, the closed-loop control of PZTs can be adopted to eliminate the hysteresis behaviors and improve the positioning accuracy of the stage. Besides, the pre-tightening methods of PZT actuator will be improved to increase the output displacement of PZT actuator and the PZT actuator with larger strokes can be adopted to obtain a larger motion range. Also, the Roll-to-Roll printing experiment will be conducted to verify the performance of error compensation, when the Roll-to-Roll Printed Electronics prototype is



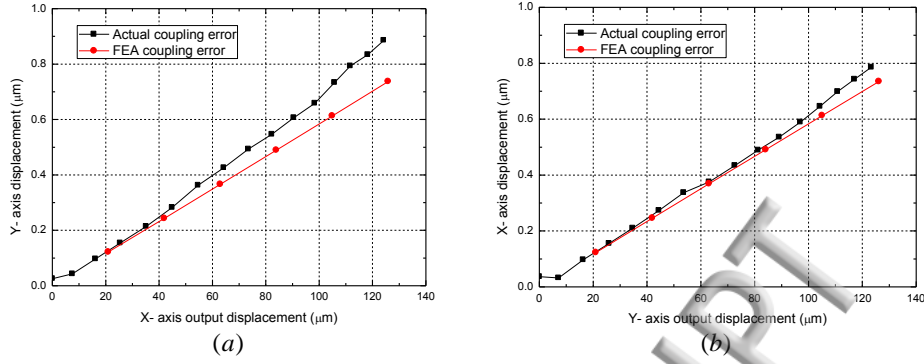


FIG. 27. Experimental results of coupling errors along  $x$ - and  $y$ - axis.

constructed.

## VI. CONCLUSION

A new decoupled flexure-based compound alignment stage is proposed for Roll-to-Roll Printed Electronic. The alignment stage consists of four key parts in a serial manner and possesses the capacity to compensate errors in 5-DOF. In the four parts, a 2-DOF parallel micropositioning stage is utilized to achieve 2-DOF decoupling motion and a two-grade displacement amplifier is adopted to enlarge the travel range of the parallel micropositioning stage. A RCM mechanism is designed with flexure hinges to avoid coupling movement and improve the alignment accuracy. Analytical models including Kinematic and static models, have been established to analyze the performance of the alignment stage, which has been verified by FEA. After the dimensional design, a prototype of the alignment stage is fabricated by the WEDM technique. Then experiments are conducted to test the prototype. The simulation and experimental results indicate that the alignment stage possesses an excellent performance with an adjusting range of  $148.11\mu\text{m} \times 149.73\mu\text{m} \times 813.61\mu\text{m} \times 1.558\text{mrad} \times 3.501\text{mrad}$  with the output coupling of 0.693% and 0.637% between  $x$ - and  $y$ - axis, which validates the effectiveness of the proposed alignment stage.

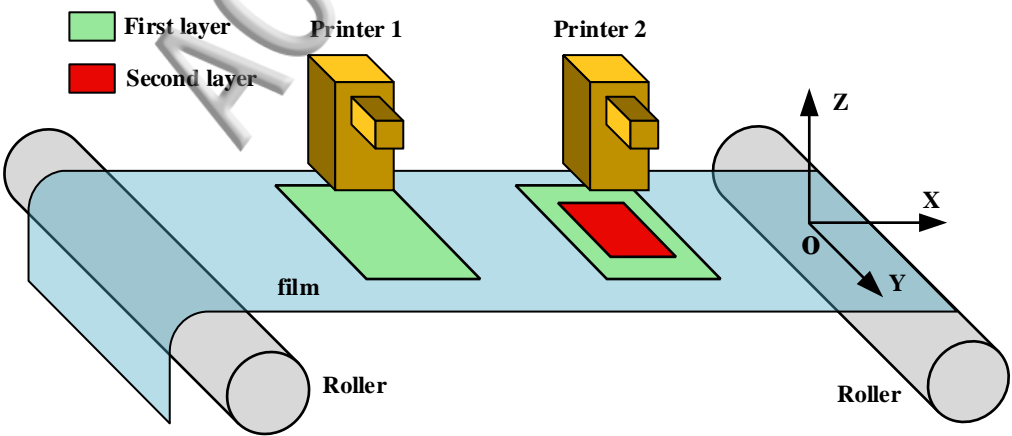
## ACKNOWLEDGMENTS

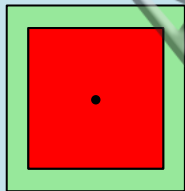
This work is financially supported by National Natural Science Foundation of China (NSFC) under Grant No. 51475017.

## REFERENCES

- <sup>1</sup>J. Virtanen, J. Virkki, U. Leena, and S. Lauri, *Advances in Internet of Things*. 2(4), 79-85 (2012).
- <sup>2</sup>L. Hu, J. W. Choi, Y. Yang, S. Jeong, F. L. Mantiaa, L. F. Cui and Y. Cui, *Proc. Natl. Acad. Sci. U. S. A.* 106(51), 21490-21494 (2009).
- <sup>3</sup>V. Subramanian, J. B. Lee, V. H. Liu, and S. Moles, in *2006 IEEE International Solid State Circuits Conference - Digest of Technical Papers*(IEEE, San Francisco, 2006) PP.1052-1059.
- <sup>4</sup>V. Kantola, J. Kulovesi, L. Lahti, R. Lin, M. Zavodchikova, and E. Coatanea, *Bit Bang*. 63-102 (2009).
- <sup>5</sup>Angelo and Peter, University of Toronto (2013).
- <sup>6</sup>L. E. Murr, *3D Printing: Printed Electronics*. Springer International Publishing. 613-628 (2015).
- <sup>7</sup>N. Genina, D. Fors, H. Vakili, P. Ihalainen, L. Pohjala, H. Ehlers, I. Kassamakov, E. Haeggstrm, P. Vuorela, J. Peltonen, and N. Sandler, *Eur. J. Pharm. Sci.* 47(3), 615-623 (2012).
- <sup>8</sup>M. Allen, C. Lee, B. Ahn, T. Kololuoma, K. Shin, and S. Ko, *Microelectron. Eng.* 88(11), 3293-3299 (2011).
- <sup>9</sup>P. Harrop, IDTechEx Report (2012).
- <sup>10</sup>H. Kopola, E. Hurme, J. M. Kuusisto, M. Smolander, M. Tuomikoski, T. Kololuoma, et al., VTT Report (2007).
- <sup>11</sup>F. C. Krebs, *Sol. Energy Mater. Sol. Cells*. 93(4), 394-412 (2009).
- <sup>12</sup>A. Seshadri, P. R. Pagilla and J. E. Lynch, *J. Dyn. Syst., Meas., Control*. 135(3), 031016 (2013).
- <sup>13</sup>C. Branca, P. R. Pagilla and K. N. Reid, *J. Dyn. Syst., Meas., Control*. 135(1), 011018 (2013).
- <sup>14</sup>C. H. Kim, J. Jo and S. H. Lee, *Rev. Sci. Instrum.* 83(6), 065001 (2012).
- <sup>15</sup>C. H. Kim, H. I. You, and J. Jo, *Jpn. J. Appl. Phys.* 52(5S1), 05DB08 (2013).
- <sup>16</sup>H. K. Kang, C. W. Lee, and K. H. Shin, *J. Process Control*. 20(5), 643-652 (2010).
- <sup>17</sup>H. K. Kang, C. W. Lee, and K. H. Shin, *IFAC Proc. Vol.* 44(1), 6763-6770 (2011).
- <sup>18</sup>Z. Chen, H. Jiang, Y. Qian, W. Yu, Q. Jing, *Proc. Int. Conf. on IEA*, 689-697 (2012).

- <sup>19</sup>Y. K. Yong, T. F. Lu, and D. C. Handley, *Precis. Eng.* 32(2), 63-70 (2008).
- <sup>20</sup>X. Xiao, Y. M. Li, and S. L. Xiao, *Microsyst Technol.* 1-11 (2016).
- <sup>21</sup>S. C. Wan, Y. L. Zhang, and Q. S. Xu, *Proc. Inst. Mech. Eng., Part C.* 0954406216643341 (2016).
- <sup>22</sup>P. Baldesi, *Mass. Inst. Technol.* 102-104 (2009).
- <sup>23</sup>Y. Zhu, *Mass. Inst. Technol.* 79-80 (2009).
- <sup>24</sup>J. Zhao, H. Wang, R. Gao, P. Hu and Y. Yang, *Rev. Sci. Instrum.* 83, 065102 (2012).
- <sup>25</sup>X. Zhou, J. Cheng, N. Zhao, and S. Chen, *Proc. of the Annual Meeting of the ASPE Saint Paul, MN, USA.* 353-357 (2013)
- <sup>26</sup>X. Zhou, H. Xu, J. Cheng, N. Zhao and S. Chen, *Sci. Rep.* 5 (2015)
- <sup>27</sup>S. H. Chang, B. C. Du, *Rev. Sci. Instrum.* 69(4), 1785-1791 (1998).
- <sup>28</sup>E. Sarajlic, C. Yamahata, M. Cordero, H. Fujita, *J. Microelectromech. Syst.* 19(2), 338-349 (2010).
- <sup>29</sup>L. L. Howell, *Compliant Mechanisms* (Wiley, New York, 2001).
- <sup>30</sup>E. Sarajlic, C. Yamahata, M. Cordero, and H. Fujita, *J. Microelectromech. Syst.* 19, 338349 (2010).
- <sup>31</sup>M. Stranczl, E. Sarajlic, H. Fujita, M. A. M. Gijs, and C. Yamahata, *J. Microelectromech. Syst.* 21(3), 605-620 (2012).
- <sup>32</sup>N. Lobontiu, *Compliant Mechanisms: Design of Flexure Hinges* (CPR Press, Boca Raton, FL, 2002).





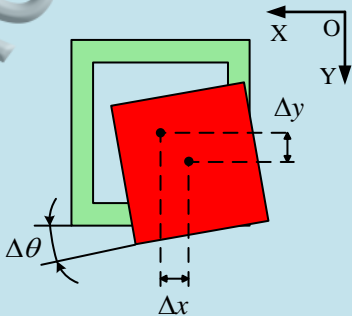
Precise alignment



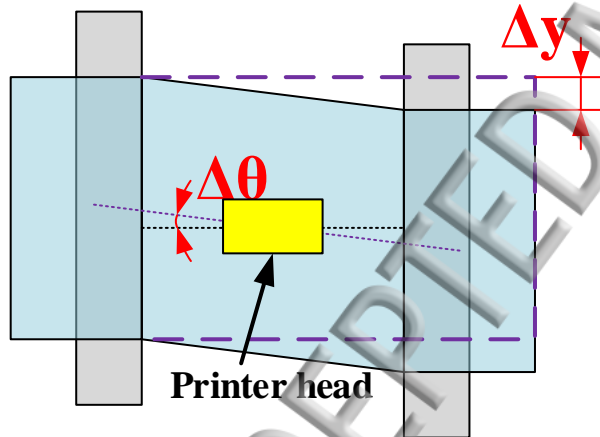
First layer



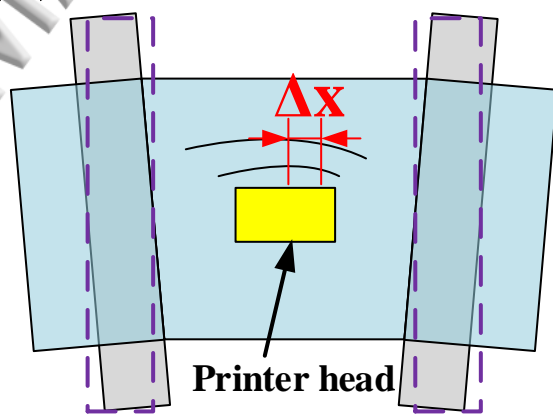
Second layer



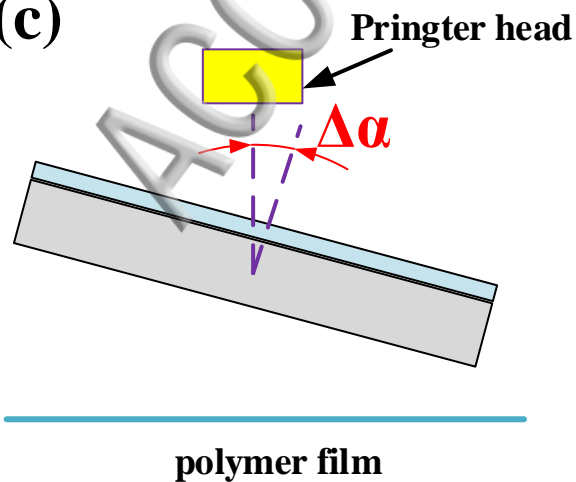
**(a)**



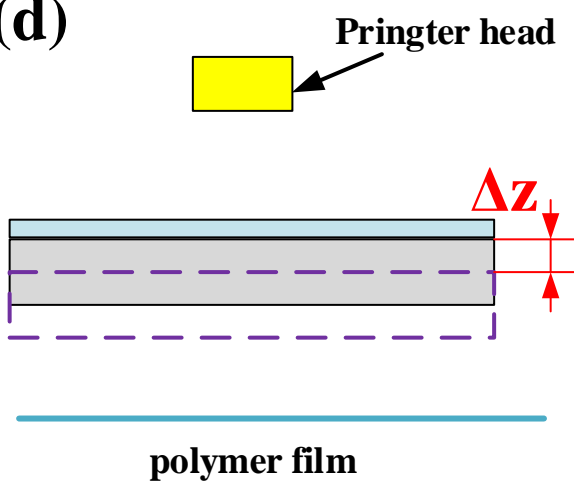
**(b)**



**(c)**

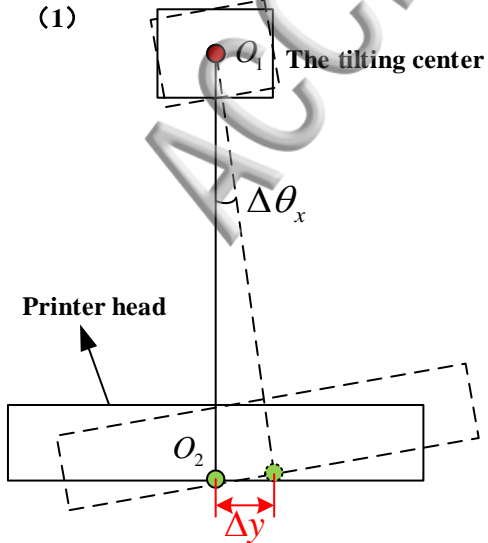


**(d)**

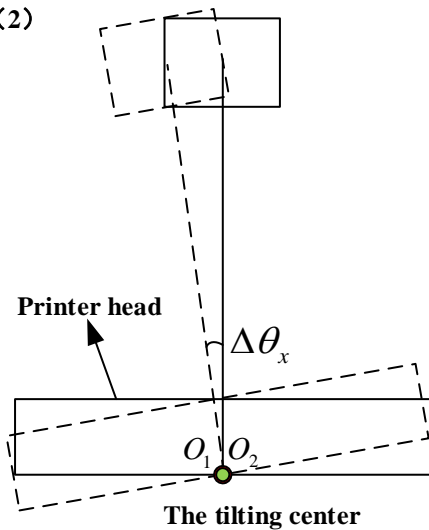


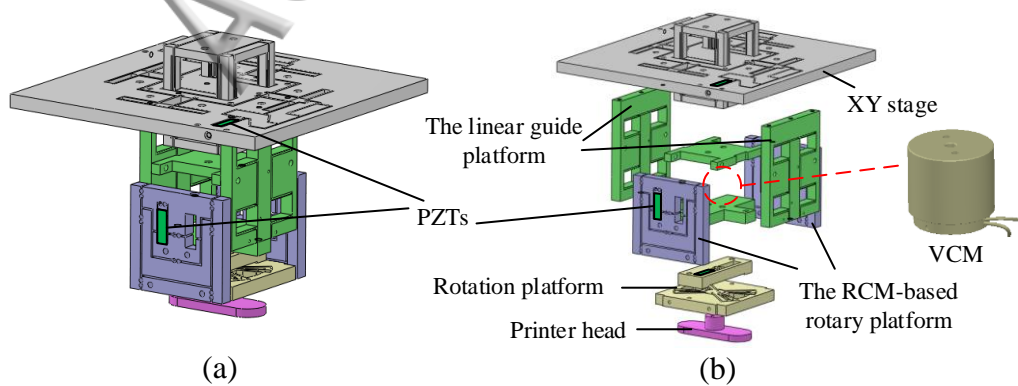


(1)



(2)





ACCEPTED

Two-grade  
displacement amplifier

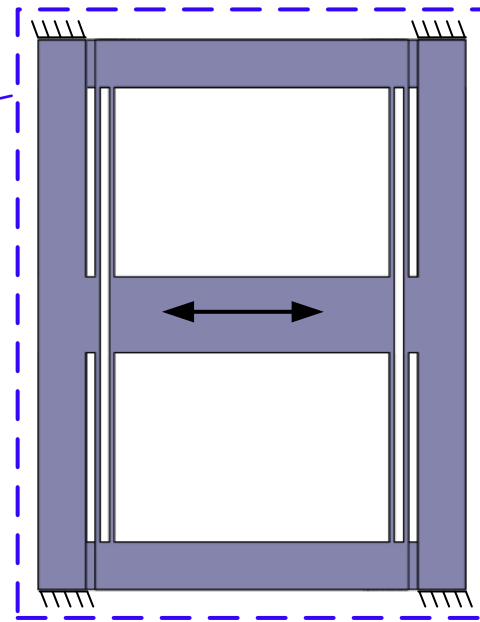
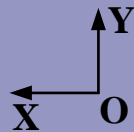
PZT

Module A

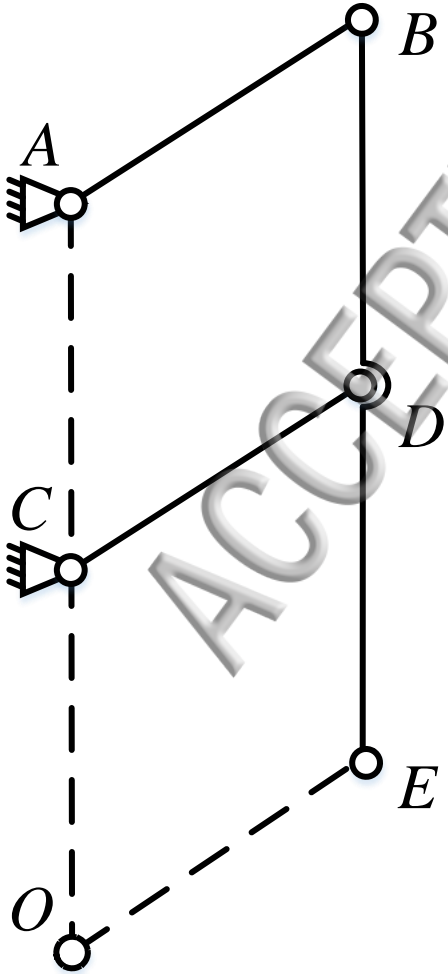
PZT

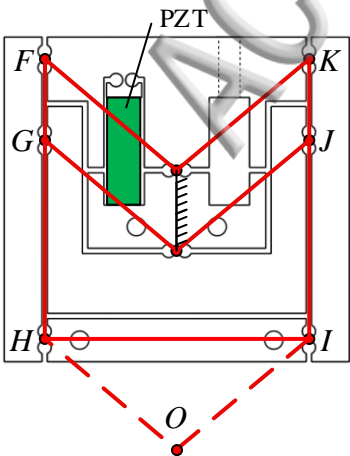
Module B

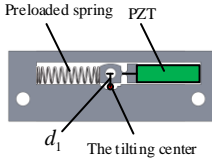
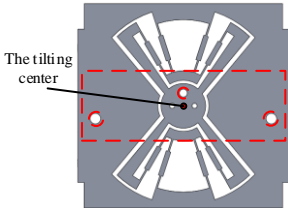
$F_{in}$



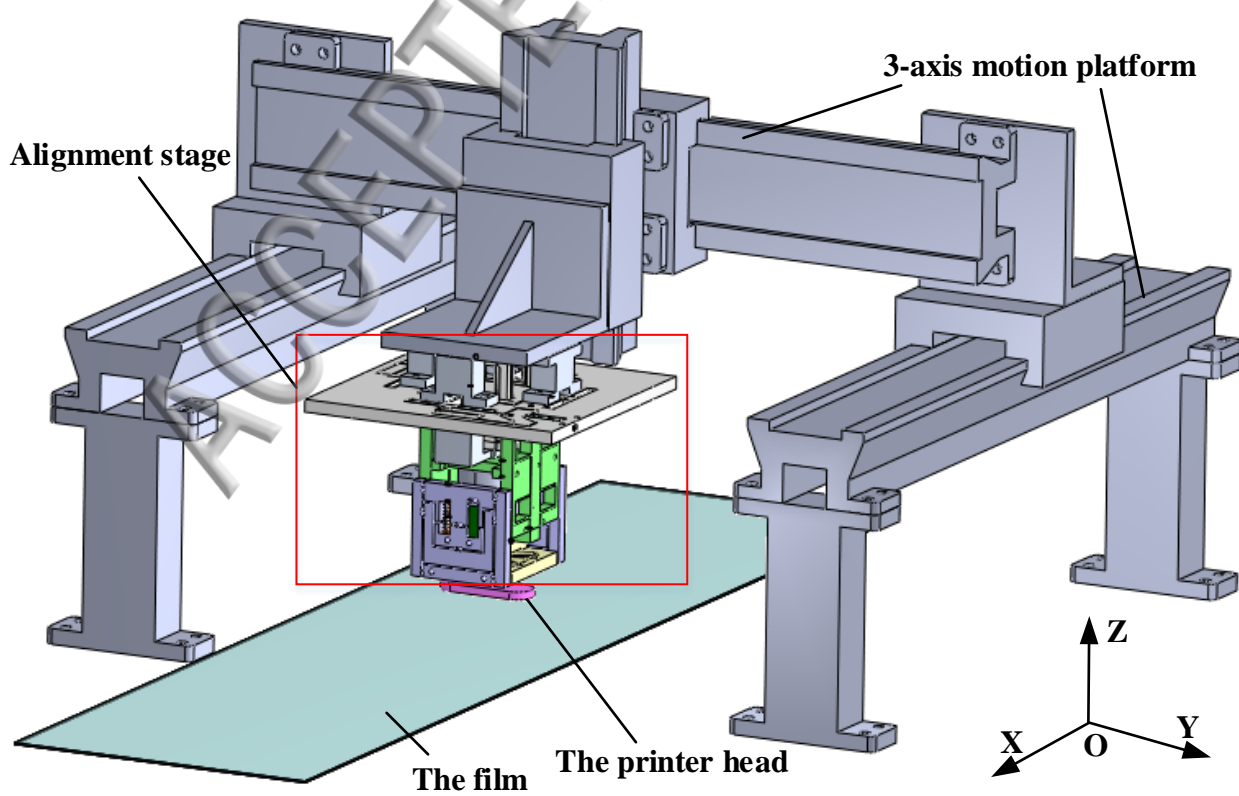
Module C

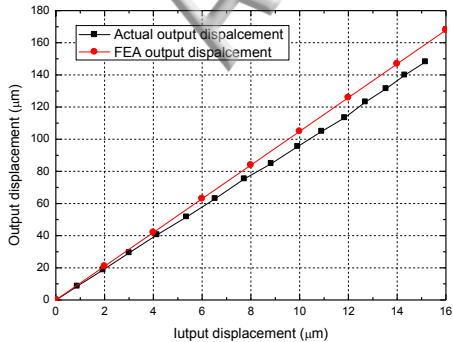




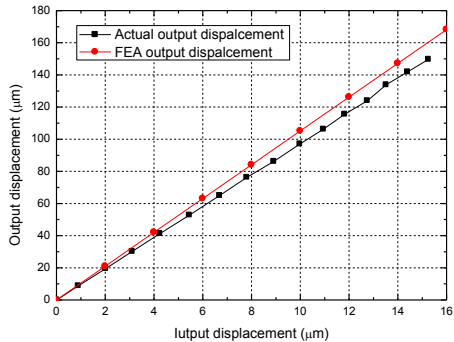




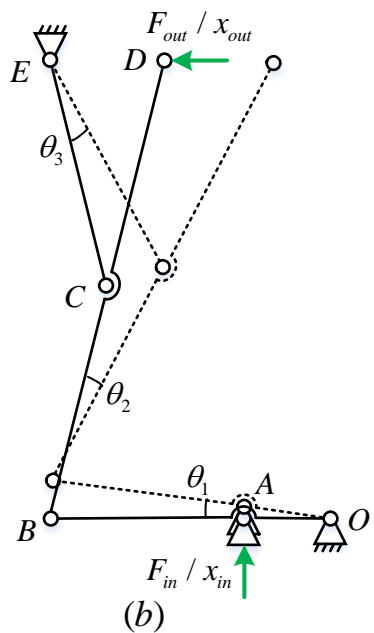
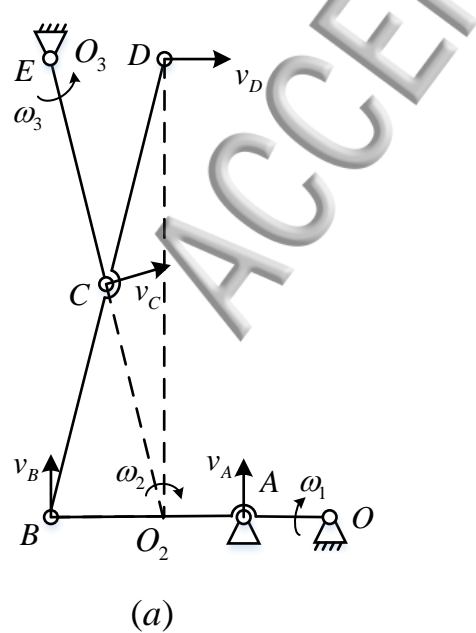


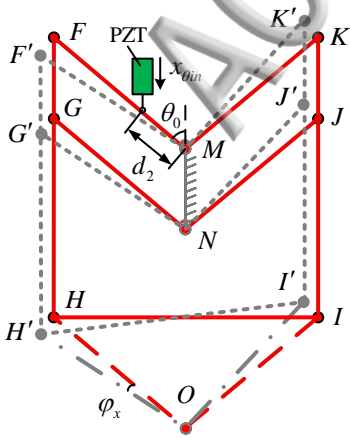


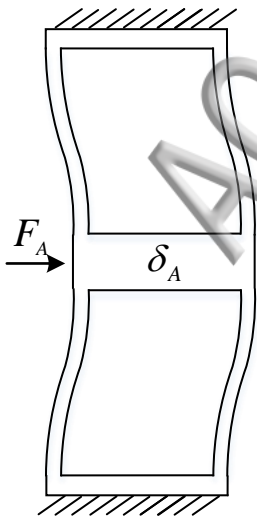
(a)



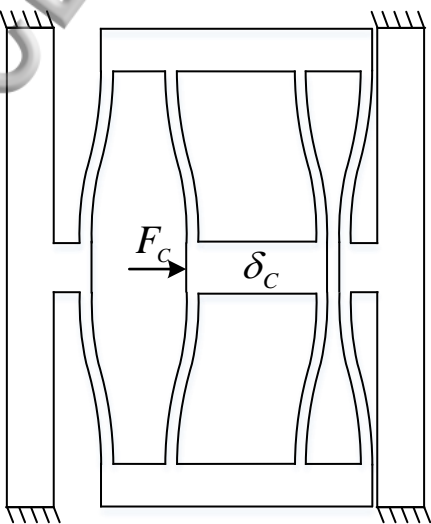
(b)



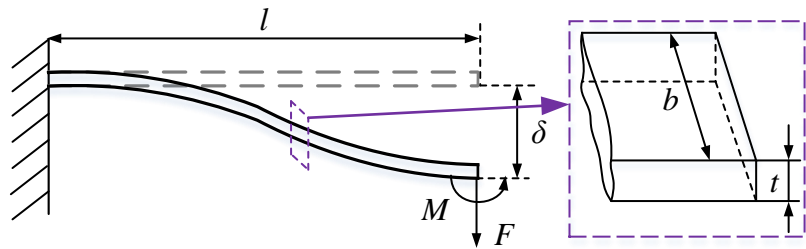




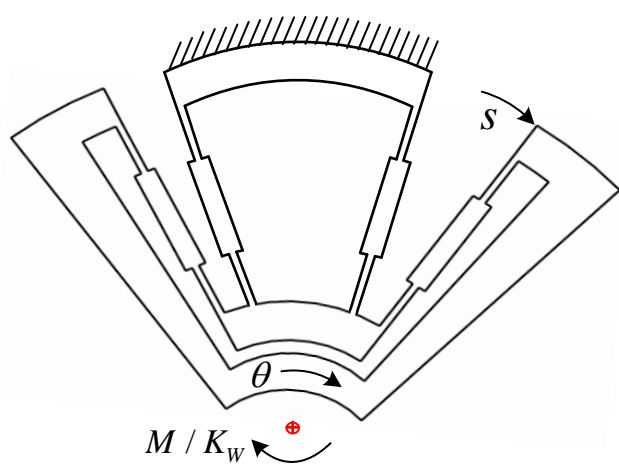
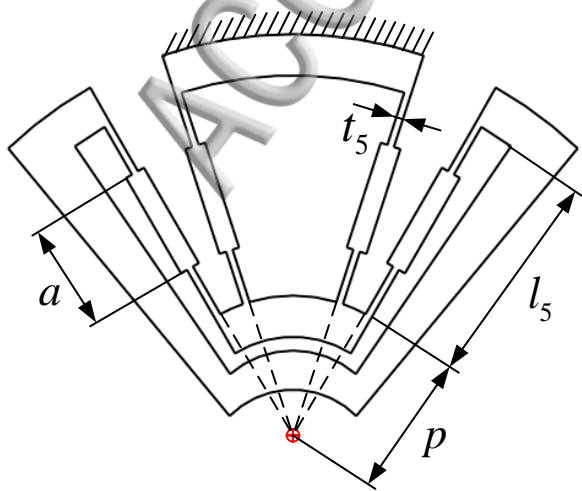
*Module A*



*Module C*







**A: Static Structural**

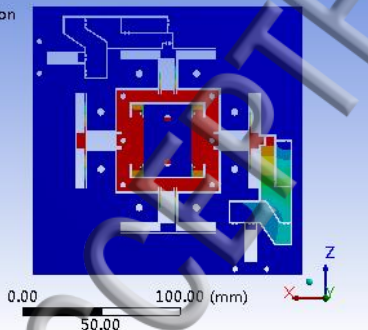
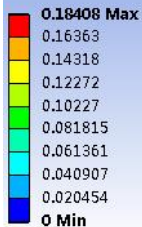
Total Deformation

Type: Total Deformation

Unit: mm

Time: 1

2016/7/16 16:41



(a)

**A: Static Structural**

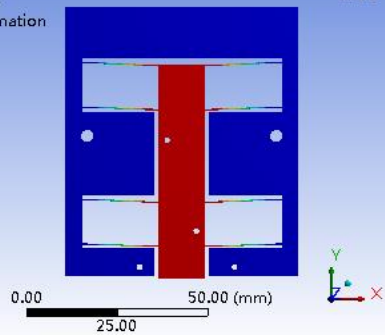
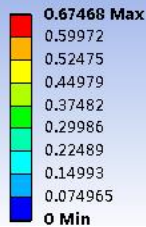
Total Deformation

Type: Total Deformation

Unit: mm

Time: 1

2016/7/16 16:59



(b)

**A: Static Structural**

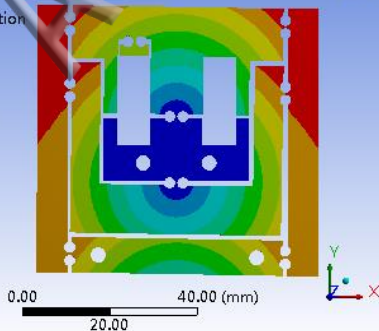
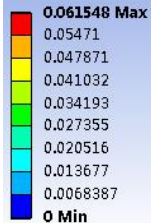
Total Deformation

Type: Total Deformation

Unit: mm

Time: 1

2016/7/16 17:07



(c)

**A: Static Structural**

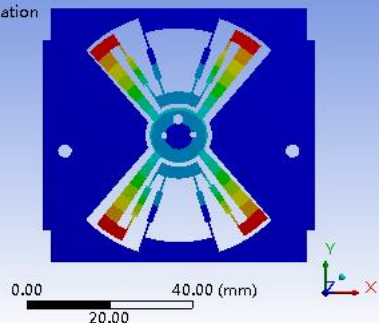
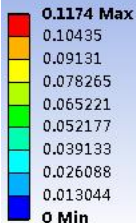
Total Deformation

Type: Total Deformation

Unit: mm

Time: 1

2016/7/16 17:19



(d)

**A: Static Structural**

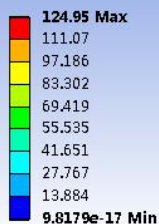
Equivalent Stress

Type: Equivalent (von-Mises) Stress

Unit: MPa

Time: 1

2016/7/18 11:05



(a)

**A: Static Structural**

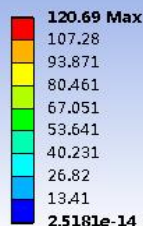
Equivalent Stress

Type: Equivalent (von-Mises) Stress

Unit: MPa

Time: 1

2016/7/18 11:11



(b)

**A: Static Structural**

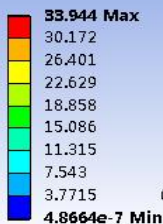
Equivalent Stress

Type: Equivalent (von-Mises) Stress

Unit: MPa

Time: 1

2016/7/18 11:08



(c)

**A: Static Structural**

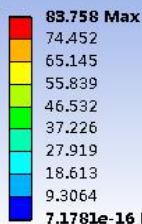
Equivalent Stress

Type: Equivalent (von-Mises) Stress

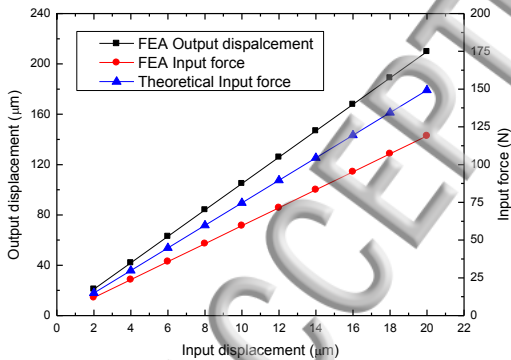
Unit: MPa

Time: 1

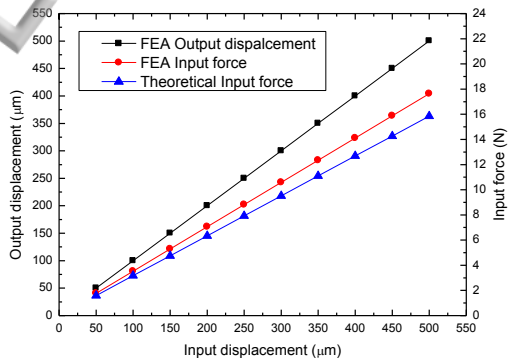
2016/7/18 11:17



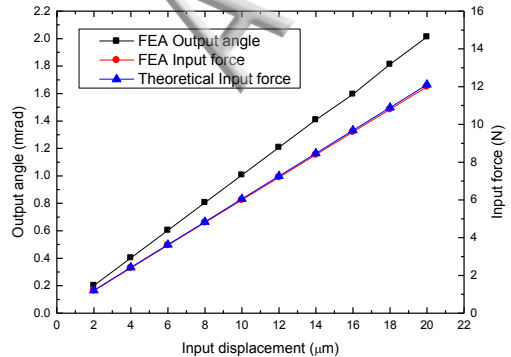
(d)



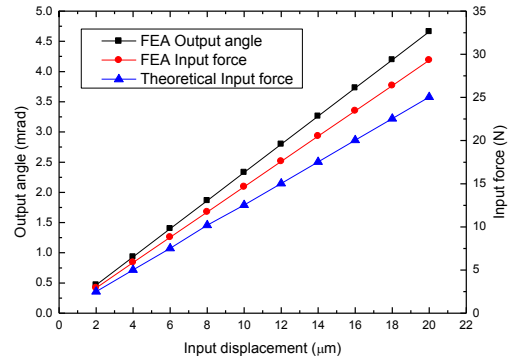
(a)



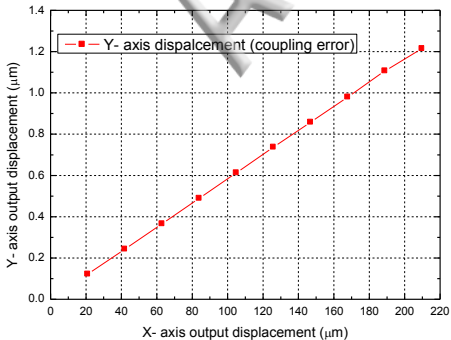
(b)



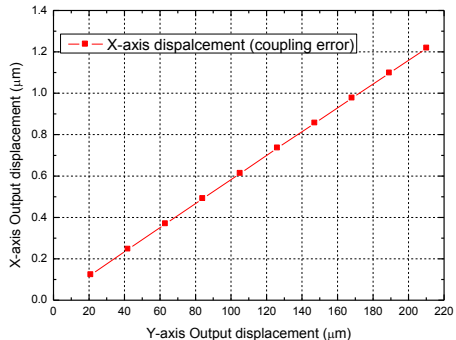
(c)



(d)

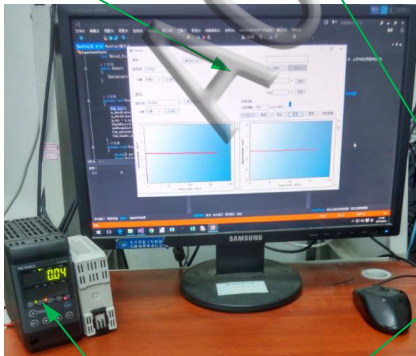


(a)

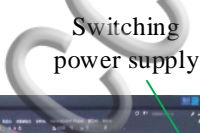


(b)

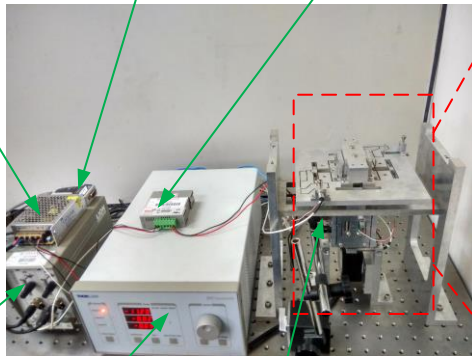
PC



Switching  
power supply



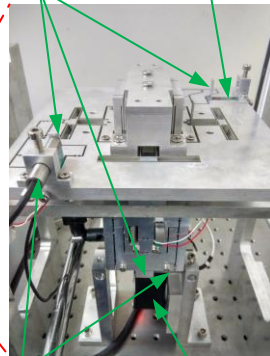
Linear encoder  
alignment tool



Elmo VCM  
controller

Measured target

PZT



Alignment tool

Capacitive sensor  
controller

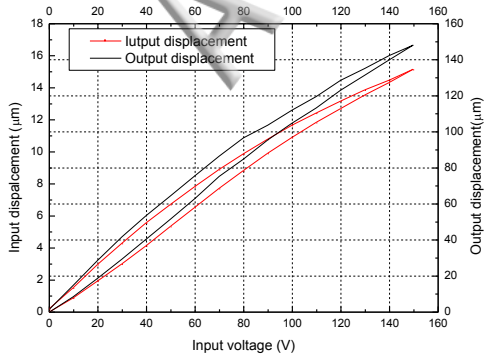
Piezo controller

Linear encoder  
sensor head

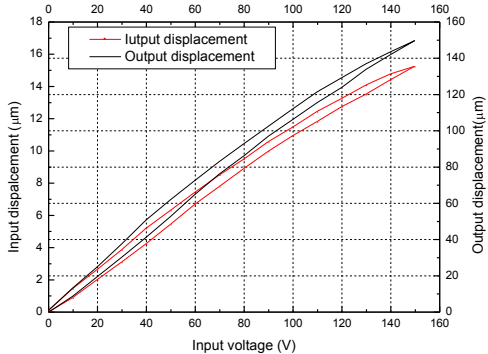
Capacitive  
sensor probe

Laser sensor  
head

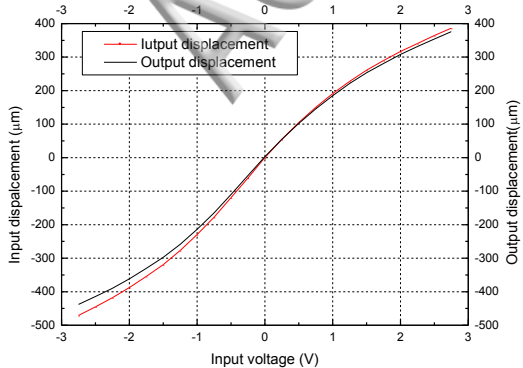




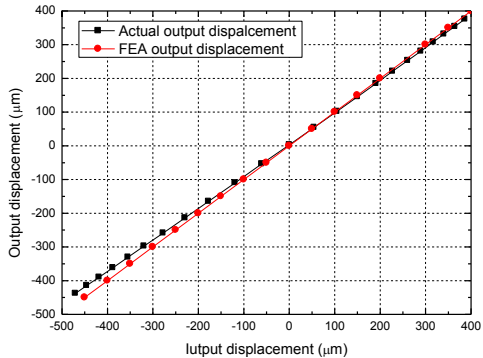
(a)



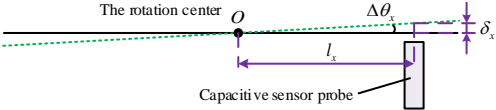
(b)

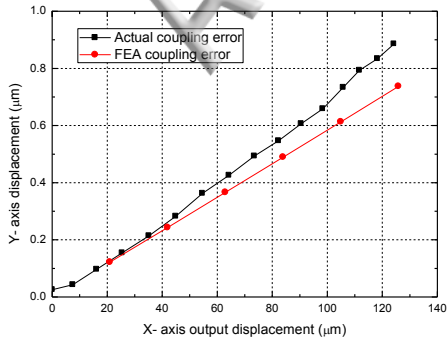


(a)

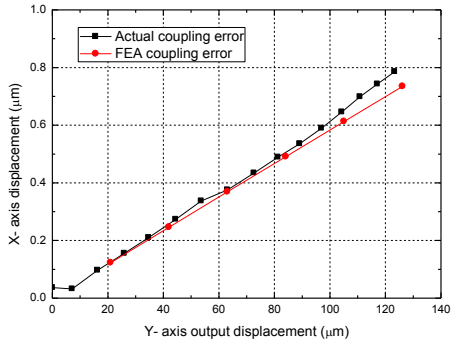


(b)

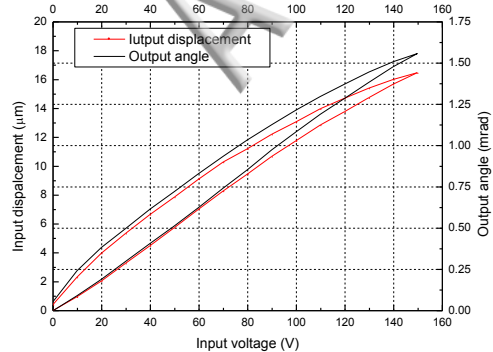




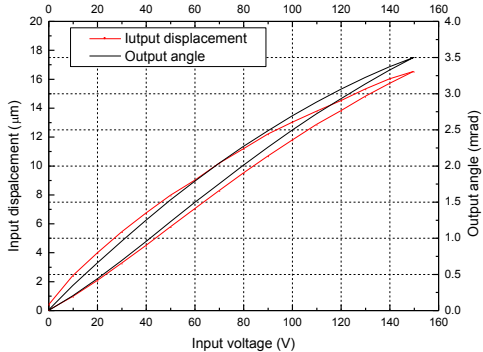
(a)



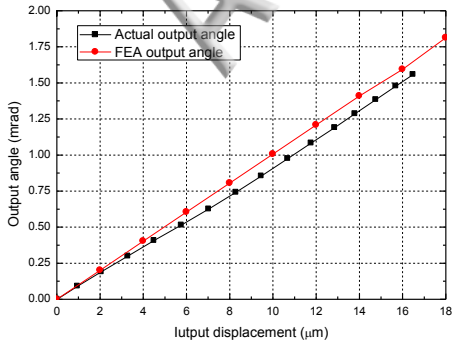
(b)



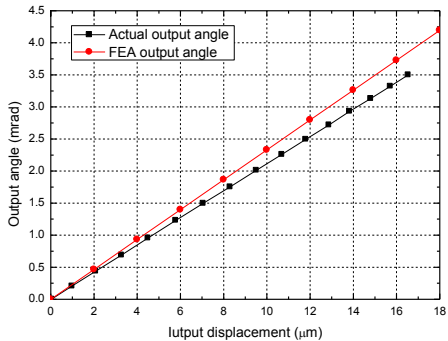
(a)



(b)



(a)



(b)